IRWIN AND JOAN JACOBS
CENTER FOR COMMUNICATION AND INFORMATION TECHNOLOGIES

An Information Theoretic View of Distributed Antenna Processing in Cellular Systems

Oren Somekh, Osvaldo Simeone, Yeheskel Bar-Ness, Alexander M. Haimovich, Umberto Spagnolini and Shlomo Shamai (Shitz)

CCIT Report #672
December 2007

DEPARTMENT OF ELECTRICAL ENGINEERING
TECHNION - ISRAEL INSTITUTE OF TECHNOLOGY, HAIFA 32000, ISRAEL

CCIT Report #672 November 2007

PUBLISHED IN: "DISTRIBUTED ANTENNA SYSTEMS:
OPEN ARCHITECTURE FOR FUTURE WIRELESS COMMUNICATIONS"

Chapter 1

An Information Theoretic View of Distributed Antenna Processing in Cellular Systems

Oren Somekh, Osvaldo Simeone, Yeheskel Bar-Ness, Alexander M. Haimovich - New-Jersey Institute of Technology
Umberto Spagnolini - Politecnico di Milano
Shlomo Shamai (Shitz) - Technion, Israel Institute of Technology

This chapter presents a survey of information theoretic results available on DAS in cellular systems. The treatment focuses on the derivation of the sum-rate of different inter-cell and intra-cell communications strategies for both uplink and downlink. A simple symmetric family of cellular models in which the inter-cell interferences are emerging from a the adjacent cells only is considered. Although hardly realistic, this family of models accounts for essential parameters of cellular systems such as inter-cell interference and fading. Whenever computation of the sum-rate is intractable or yields little insight into the problem, asymptotic performance criteria (e.g. extreme-SNR parameters) are evaluated. Emphasis is placed on the assessment of benefits of cooperation among APs (i.e. joint detection/precoding).

Mathematical tools underlying the results are introduced briefly where necessary. Finally, some advanced topics, such as cooperation among terminals, are discussed as well.

1.1 Introduction

Information theory provides a solid reference framework for a thorough understanding of communication systems. An accurate information theoretic enables to assess the limiting performance expected by a given technology and to yield insight into practical design solutions.

From an information theoretical standpoint, distributed antenna systems (DAS) qualify as either a vector multiple access channel (MAC) or a broadcast channel (BC), according to whether the uplink or downlink are considered. The limiting performance (capacity region) and optimal transmission/reception schemes for such scenarios have been widely studied under both Gaussian and fading channels (e.g., [1] [2] [3]). However, the distributed nature of DAS provides the analysis of this system with a unique structure that deserves a separate treatment. In particular, the main differences between the *micro-diversity* provided by the use of conventional collocated antenna arrays and the *macro-diversity* provided by DAS, reduces to (*i*) the power profile of the resulting channels transfer matrices; (*ii*) the power constraints; (*iii*) possible limitations on the capacity of links (i.e., the *backbone*) connecting access points (APs) to the *central processing unit*. These points are elaborated upon in the following.

(*i*) The channel transfer matrix describes the complex channel propagation gains between each pair of transmit and receive antennas. With antenna array systems (micro-diversity), the entries of the channel matrix can be modeled as identically distributed, since the elements of the antenna arrays are collocated, and thus experience similar propagation conditions. This enables the use of standard analytical tools from random matrix theory [4]. In contrast, with DAS (macro-diversity), the channel gains between any terminal and the distributed antennas of the APs may have different statistics, as dictated by the characteristics of propagation, such as path loss, shadowing, line-of-sight components, and the system

topology. It follows that, in general, the power profile of the corresponding channel matrix is non-uniform, preventing a simple application of known tools to the scenario at hand.

(*ii*) For collocated antenna arrays, power constraints are generally imposed on the sum-power radiated by all the elements of the array. Conversely, for distributed APs, since each element is provided with a separate power amplifier, the constraints have to be enforced on a per-AP basis. This creates specific challenges in pursuing an analytical treatment of DAS.

(*iii*) Different APs in a DAS are connected through high capacity links (referred to as the backbone) to a central processing unit, which jointly processes the signals transmitted/received by the APs. Though the backbone is generally composed of highly reliable wireline links (e.g., optical fibers), delay and/or locality constraints may have to be considered, especially in large DAS. This feature is radically different from the centralized processing available at little cost in collocated antenna arrays.

The system layout in DAS is likely to present distributed and regularly displaced APs according to a cellular structure. This structure can be effectively captured by a somewhat simplistic model, referred to in the literature as Wyner's model, and first presented in the context of multicell networks in [5] [6]. In this model, inter-cell interference is limited to adjacent cells and is measured by a single parameter α (see Fig. 1.1 and 1.2). The model is simple enough to allow, to a certain extent, analytical treatment, but also sufficiently rich to incorporate the main features of propagation in DAS.

This chapter presents a survey of the information theoretic results available on the uplink and downlink of DAS under the Wyner model for Gaussian and fading channels. The treatment aims at presenting the main analytical results concerning both the ultimate performance of the system (under optimal transmission/reception schemes) and limitations of suboptimal solutions. Furthermore, recent results that attest to the advantages of employing cooperative technology among terminals are briefly discussed.

The rest of the chapter is organized as follows. Sec. 1.2 introduces the Wyner cellular model along with the transmission/reception schemes of interest and the performance criteria employed in the analysis throughout the chapter. The uplink of a Wyner's model

is investigated in Sec. 1.3, while the corresponding study of downlink is covered in Sec. 1.4. The advantages of cooperation among terminals are studied in Sec. 1.5. Concluding remarks and related open problems are included in Sec. 1.6. Finally, a bibliographical notes are presented in Sec. 1.7.

1.2 System Model

In this section, we present the framework under which the results of this chapter are formulated. In particular, Sec. 1.2.1 introduces the physical model describing the relationship between the signal transmitted by the mobiles and received by the base stations (uplink) or, dually, transmitted by the base stations and received by the mobiles (downlink). Sec. 1.2.2 introduces the main transmission/reception schemes of interest, whose performance is evaluated and compared throughout the chapter. Finally, performance criteria used throughout this chapter are briefly described in Sec. 1.2.2.

1.2.1 Wyner's Model

A family of physical models that prescribes that each cell senses only signal radiated form a limited number of neighboring cells has been introduced by by Hanly and Whiting in [5] and by Wyner in [6]. For instance, the basic *linear* model, depicted in Fig. 1.1, consists of a linear array of M identical cells with single antenna base-stations. The K single antenna users contained in each cell, "see" only their own cell-site antenna and the two adjacent cell-site antennas. The flat fading experienced by the users is assumed independent identically distributed (i.i.d.) among different users and ergodic in the time index. As a further simplification, the path loss (i.e., the average fading power) towards adjacent cells is represented by a single parameter $\alpha \in [0, 1]$. Although this model is simplistic, it encompasses the impact of central factors of a cellular system and accounts for phenomena like fading and inter-cell interference.

As a result of the assumptions discussed above, the overall channel transfer matrix of

these models (to be rigorously defined in the sequel) consists of finite number of non-zero diagonals regardless of the matrix dimensions. This fact precludes the use of results in the field of random matrices, which were recently used successfully for calculating the sum-rates of several interesting communication setups [4]. Nevertheless, the simplicity of the Wyner model family renders analytical treatment feasible, which in turn provides much insight and understanding of DAS.

The basic linear Wyner's model in Fig. 1.1 will be considered in the rest of the chapter for its simplicity, in order to get insight into the role of different system and channel parameters in the system overall performance. However, extension to more complex (and realistic) scenarios is conceptually straightforward, and results will be mentioned in the following, whenever available. Among interesting generalizations of the model that have been considered in the literature, we recall:

- *Circular model*: in several cases of interest it is convenient to assume that the M cells are arranged on a circle. In this setup, introduced in [5], the first and last indexed cells are adjacent, resulting in a perfectly symmetric and homogenous model with no boundary effects. It is noted that in the limit where the number of cells goes to infinity the boundary effects are negligible, both linear array and circular array models are "equivalent" under the performance merits of interest.

- *Planar model*: a finite two dimensional hexagonal array is considered in [6]. In this case each cell "sees" the signal radiated in the six adjacent cell sites. Since it is assumed that the path loss is independent of the user's position, by scaling the vertical axis by a factor of $1/\sqrt{3}$, rotating the plane by 45°, and scale it by a factor of $1/\sqrt{2}$, the hexagonal array is transformed into a rectangular $M \times M$ cell array, as depicted in Fig. 1.2.

- *Cell clusters*: cells are divided into non-overlapping independent clusters with separate backbone networks and central processing units. This model is a first step towards introducing practical constraints on the backbone connecting different APs. In particular, only signals relative to APs within a cluster are jointly processed by the corresponding central processing unit, which is unaware of outer users' codebooks [7] [8].

1.2.2 Transmission/Reception Schemes of Interest

DAS inherently refers to schemes where signals either transmitted or received by the APs are jointly processed in order to enhance the system performance. We refer to this scenario as *multi-cell processing* (MCP), and distinguish it from *single-cell processing* (SCP). With SCP, each AP processes the signal (transmitted or received) independently from other, interfering, APs or users. Throughout the chapter, it is assumed that all APs and users are fully synchronized. Being a defining feature of DAS, this chapter will be devoted mostly to the study of multi-cell processing, even though, for reference, single-cell processing will be considered as well. The taxonomy of schemes of interest further divides the transmission/reception techniques according to the strategy employed at both an inter-cell and intra-cell level. This point is elaborated upon in the following.

Single-cell processing

In single-cell processing, signals radiated within other cells are considered as interference by any given AP. As far as *intra-cell* strategies are concerned, possible alternatives include:

- Orthogonal intra-cell medium access: in this case, only one user per cell is active in the considered time-frequency resource. Therefore, no intra-cell interference is produced and single-user transmission/reception strategies are used at each AP. In accordance to the literature on the subject, this solution will be referred in the following as *intra-cell TDMA*;
- Non-orthogonal intra-cell medium access: here, different users of the same cell access the time-frequency resource simultaneously, thus causing interference on the concurrent transmissions. Each AP employs multi-user processing techniques (e.g., in uplink, multi-user detection (MUD)) in order to cope with intra-cell interference. Following the literature, we will refer to this scenario as *intra-cell wide-band* (WB);
- Collaborative transmission: same-cell users cooperate for the transmission/reception of each other's data through, e.g., relaying or more sophisticated forms of cooperative

coding [9]. This situation can coexist with either orthogonal or non-orthogonal intra-cell medium access. We will consider this advanced intra-cell strategy in some detail in Sec. 1.5.

A simple solution that is commonly employed in cellular systems in order to reduce interference is that of using the same channel (i.e., frequency or time resource) only in cells sufficiently separated. This *inter-cell* strategy is usually referred to as frequency reuse, and in Wyner's model allows to totally eliminate inter-cell interference. For instance, in the linear model, it is enough to activate odd cells in orthogonal channels (in either time or frequency) with respect to even cells in order to have inter-cell interference-free communications. This scenario is referred to in the literature as *inter-cell time-sharing* (ICTS).

Multi-cell processing

As explained above, multi-cell processing is a defining feature of DAS, and is based on joint processing of all the signals transmitted or received by the APs. To simplify the analysis, and putting focus on ultimate bounds, here an ideal delayless, infinite capacity "backbone" network is assumed to connect all APs to a central unit, which jointly processes all the signals. Alleviating this assumption is the subject of a number of recent publications [10] [11]. The central unit is aware of all the users' codebooks and their channel state information (CSI). Finally, for the downlink, the users are assumed to be aware only of their own CSI and codebooks. Intra-cell strategies are defined as above. Notice that APs here always employ multi-user transmission/reception strategies.

Performance criteria

Throughout the chapter, the performance of different schemes and scenarios is evaluated in terms of *per-cell ergodic sum-rate* (measured in $nats/s/Hz$ or $bit/s/Hz$) [1]. This performance criterion is well suited for fading channels that vary fast enough so as to allow each

[1] Due to the symmetry of the system model, the per-cell sum-rate divided by the number of users per cell is a reliable measure of the rate achieved by each user.

transmitted codeword to experience a large number of fading states, while it is in general not appropriate for delay sensitive applications. For the uplink, since each user has a separate power amplifier, a per-user power constraint of P is enforced, which amounts to a per-cell power constraint of $\bar{P} = KP$, where K is the number of users. For the downlink, since the APs serves all the users through a single power amplifier, a per-cell power constraint of $\bar{P}$ is considered.

In cases where the ergodic sum-rate provides little insight into the performance of the system due to cumbersome analytical expressions, asymptotic measures will be considered as follows.

Extreme SNR Analysis For low signal-to-noise ratios (SNRs), the sum-rate R of a given scheme is described by the minimum transmitted energy per bit required for reliable communication (normalized to the background noise power spectral density N_0) $E_b/N_{0_{\min}}$ and by the slope S_0 at $E_b/N_{0_{\min}}$ (measured in [bit/sec/Hz/(3 dB)]) [12]. In particular, R can be approximated by the *affine* function of E_b/N_0 measured in [dB]:

$$R \simeq \frac{S_0}{3[\text{dB}]} \left(\frac{E_b}{N_0}[\text{dB}] - \frac{E_b}{N_{0\,\min}}[\text{dB}] \right) \ . \tag{1.1}$$

The low-SNR characterization in terms of parameters $E_b/N_{0_{\min}}$ and S_0 turns out to depend on both the first ($\dot{R}(\text{SNR})$) and second ($\ddot{R}(\text{SNR})$) derivatives of the achievable rate $R(\text{SNR})$ when measured in [nats/sec/Hz] [12]. In fact, it can be shown that:

$$\frac{E_b}{N_{0\,\min}} = \frac{\log 2}{\dot{R}(0)} \tag{1.2a}$$

$$S_0 = \frac{2[\dot{R}(0)]^2}{-\ddot{R}(0)} \ . \tag{1.2b}$$

In the high-SNR regime, the sum-rate of a given scheme can be expanded as an *affine* function of the SNR (measured in [dB]) [13]:

$$R \simeq S_\infty \left(\frac{\text{SNR}[\text{dB}]}{3[\text{dB}]} - \mathcal{L}_\infty \right) \ , \tag{1.3}$$

where the high-SNR parameters S_∞ (slope or multiplexing gain measured in [bits/sec/Hz/(3 dB)] and $\mathcal{L}_\infty$ (power offset measured in 3 [dB] units with respect to a reference channel having the same slope but with zero power offset), read:

$$S_\infty = \lim_{\mathrm{SNR}\to\infty} \frac{R}{\log_2 SNR} \tag{1.4}$$

$$\mathcal{L}_\infty = \lim_{\mathrm{SNR}\to\infty} \left(\log_2 \mathrm{SNR} - \frac{R}{S_\infty} \right). \tag{1.5}$$

where R is measured in [nats/sec/Hz] and in [bits/sec/Hz], in (1.4) and (1.5) respectively. If the multiplexing gain is zero, then a given scenario is said to be *interference-limited*.

Scaling Law with the Number of Users In order to study the ability of a multi-user system as DAS to profit from different fading conditions across the users of the system (multi-user diversity), it is customary to evaluate the scaling law of the sum-rate with respect to the number of users K. In particular, it is known that, for Rayleigh fading, optimality with respect to this criterion is achieved if

$$\lim_{K\to\infty} \frac{R}{\log\log K} = 1 \ , \tag{1.6}$$

indicating that the scaling law is $\log\log K$ [14].

Finally, it is noted that a *natural logarithm* base is used throughout this chapter unless specified differently.

Spectral Efficiency Most of the curves included in this chapter represent the spectral efficiency versus the transmitted E_b/N_0. This representation is considered to be more informative than the rate versus SNR representation, especially in the low-SNR regime. The spectral efficiency $\mathsf{C}(E_b/N_0)$ is defined through the following relations: $\mathsf{C}(E_b/N_0) = C(\mathrm{SNR})$ and $\mathrm{SNR} = C(\mathrm{SNR})E_b/N_0$.

1.3 The Uplink Channel

Consider the uplink of a Wyner's linear model with M cells as in Fig. 1.1. The $M \times 1$ vector baseband representation of the signals received at all cell-sites is given for an arbitrary time index by

$$\boldsymbol{y} = \boldsymbol{H}\boldsymbol{x} + \boldsymbol{z} \ , \tag{1.7}$$

where $\boldsymbol{x}$ is the $MK \times 1$ complex Gaussian symbols vector $\boldsymbol{x} \sim \mathcal{CN}(\boldsymbol{0}, P\boldsymbol{I}_{MK})$ ($\boldsymbol{I}_N$ is an $N \times N$ unity matrix), $\boldsymbol{z}$ is the $M \times 1$ complex Gaussian additive noise vector $\boldsymbol{z} \sim \mathcal{CN}(\boldsymbol{0}, \boldsymbol{I}_M)$, and $\boldsymbol{H}$ is the $M \times MK$ channel transfer matrix, given by

$$\boldsymbol{H} = \begin{pmatrix} \boldsymbol{a}_0 & \alpha\boldsymbol{c}_0 & \boldsymbol{0} & \cdots & \boldsymbol{0} & \boldsymbol{0} \\ \alpha\boldsymbol{b}_1 & \boldsymbol{a}_1 & \alpha\boldsymbol{c}_1 & \boldsymbol{0} & \cdots & \boldsymbol{0} \\ \boldsymbol{0} & \alpha\boldsymbol{b}_2 & \boldsymbol{a}_2 & \alpha\boldsymbol{c}_2 & \ddots & \vdots \\ \vdots & \boldsymbol{0} & \alpha\boldsymbol{b}_3 & \ddots & \ddots & \boldsymbol{0} \\ \boldsymbol{0} & \vdots & \ddots & \ddots & \boldsymbol{a}_{M-2} & \alpha\boldsymbol{c}_{M-2} \\ \boldsymbol{0} & \boldsymbol{0} & \cdots & \boldsymbol{0} & \alpha\boldsymbol{b}_{M-1} & \boldsymbol{a}_{M-1} \\ \end{pmatrix} \ , \tag{1.8}$$

where $\boldsymbol{a}_m$, $\boldsymbol{b}_m$ and $\boldsymbol{c}_m$, are $1 \times K$ row vectors denoting the fading channel coefficients (i.i.d. complex Gaussian with zero mean and unit power), experienced by the K users of the m-th, $(m-1)$-th, and $(m+1)$-th cells, respectively, when received by the m-th cell-site antenna.

1.3.1 Single-Cell Processing

In this section, single-cell processing is considered. Starting with the Gaussian (i.e., non-fading) scenario and assuming $M \gg 1$ in order to make border effects negligible, it is easily shown that the per-cell sum-rate is given for the linear model by

$$R_{\text{scp}} = \log\left(1 + \frac{\bar{P}}{1 + 2\alpha^2\bar{P}}\right) \tag{1.9}$$

and for the planar model by

$$\hat{R}_{\text{scp}} = \log\left(1 + \frac{\bar{P}}{1 + 6\alpha^2\bar{P}}\right), \tag{1.10}$$

where $\bar{P} \triangleq KP$ is the average per-cell transmitted power (since a unit noise power is assumed, $\bar{P}$ is also the total cell SNR). Theses rate are achieved (not uniquely) by intra-cell TDMA protocols, where each user is transmitting $1/K$ of the time with power $\bar{P}$, or by the WB protocol with MUD, according to which all users are transmitting all the time with average power P. As expected, the rates demonstrate an interference limited behavior as $\bar{P}$ increases.

For reference, the extreme SNR characterization of single cell processing over Gaussian channels, is summarized for the linear and planar models as follows:

$$\begin{array}{lll} S_0 = \frac{2}{1+4\alpha^2} \; ; & \frac{E_b}{N_0}_{\min} = \log 2 \; ; & S_\infty = 0 \\ \hat{S}_0 = \frac{2}{1+12\alpha^2} \; ; & \frac{\hat{E}_b}{N_0}_{\min} = \log 2 \; ; & \hat{S}_\infty = 0 \; . \end{array} \tag{1.11}$$

showing the deleterious effects of inter-cell interference in both regimes.

Introducing fading, and assuming that each cell-site (say the m-th) is aware of the instantaneous channel gains a_k in vector $\boldsymbol{a}_m$ and the instantaneous interference power, the per-cell ergodic sum-rate for the WB protocol deployed in the linear model is given by

$$\begin{aligned} R^*_{\text{scp}} &= E\left\{\log\left(1 + \frac{\bar{P}\sum_{k=1}^{K}|a_k|^2}{K + \alpha^2\bar{P}\sum_{k=1}^{K}(|b_k|^2 + |c_k|^2)}\right)\right\} \\ &= E\left\{\log\left(K + \frac{1}{2}\bar{P}(S + \alpha^2 T)\right) - \log\left(K + \frac{1}{2}\bar{P}\alpha^2 T\right)\right\} \; , \end{aligned} \tag{1.12}$$

where the expectation is taken over the independent random variables S and T, defined by

$$S = 2\sum_{k=1}^{K}|a_k|^2 \quad ; \quad T = 2\sum_{k=1}^{K}(|b_k|^2 + |c_k|^2) \; . \tag{1.13}$$

For the special case of Rayleigh fading $S \sim \chi^2_{2K}$ and $T \sim \chi^2_{4K}$, where χ^2_n denotes a central chi-square distribution with n degrees of freedom. In [15] it is shown that the random variable

$W = S + \alpha^2 T$ has a density distribution function given by

$$f_W(x) = \frac{x^{3K-1}\exp\left(-\frac{x}{2\alpha^2}\right)}{2^{3K}(\alpha^2)^{2K}\Gamma(3K)}{}_1\mathcal{F}_1\left(K, 3K; \frac{1}{2}\left(\frac{1}{\alpha^2}-1\right)x\right) \quad ; \quad x \geq 0, \tag{1.14}$$

where ${}_1\mathcal{F}_1(\cdot,\cdot;\cdot)$ is the Hypergeometric function of the first kind and $\Gamma(\cdot)$ is the Gamma function. Hence, (1.12) becomes

$$\begin{aligned} R^*_{\text{scp}} = & \\ & \frac{1}{\epsilon_1}\int_0^\infty \log\left(K + \frac{1}{2}\bar{P}x\right) x^{3K-1}\exp\left(-\frac{x}{2\alpha^2}\right){}_1\mathcal{F}_1\left(K, 3K; \frac{1}{2}\left(\frac{1}{\alpha^2}-1\right)x\right)dx \\ & \qquad - \frac{1}{\epsilon_2}\int_0^\infty \log\left(K + \frac{1}{2}\alpha^2\bar{P}x\right) x^{2K-1}\exp\left(-\frac{x}{2}\right)dx, \end{aligned} \tag{1.15}$$

where $\epsilon_1 = 2^{3K}(\alpha^2)^{2K}\Gamma(3K)$ and $\epsilon_2 = 2^{2K}\Gamma(2K)$. It is noted that the sum-rate of the intra-cell TDMA is achieved by setting $K = 1$ in (1.15). To get the SCP sum-rate for the planar model replace $2K$ with $3K$, and $3K$ with $4K$ in (1.15).

Focusing on the case where $K \gg 1$ while the total transmit power $\bar{P}$ is kept constant, the strong law of large number (SLLN) can be employed to the normalized sums of (1.12). This shows that for $K \to \infty$ the rate (1.12) boils down to (1.9). Hence, for large number of users, the WB protocol demonstrates no penalty in the presence of fading. This results reflects the well known phenomenon of channel "hardening" by multi-user diversity. It is noted that the same result apply for the planar model and to a general zero-mean unit-power fading distribution.

Extreme SNR characterization of the SCP with Rayleigh fading for the linear and planar models reads

$$\begin{aligned} S_0^* = \tfrac{2}{1+4\alpha^2+\frac{1}{2K}} \; ; \quad \tfrac{E_b}{N_0}^*_{\min} = \log 2 \; ; \quad S_\infty^* = 0 \\ \hat{S}_0^* = \tfrac{2}{1+24\alpha^2+\frac{1}{2K}} \; ; \quad \tfrac{\hat{E}_b}{N_0}^*_{\min} = \log 2 \; ; \quad \hat{S}_\infty^* = 0 \; , \end{aligned} \tag{1.16}$$

showing that, for increasing K, the performance reduces to the non-fading setup (1.11).

In Fig. 1.3 the interference limited behavior of the linear model SCP spectral efficiency is

demonstrated for $\alpha = 0.4$ (which represents a situation where the overall inter-cell interference power is about third of the received useful signal power) and several values of K. The dependency of this sum-rate on α is demonstrated in Fig. 1.4 for $\bar{P} = 10$ [dB] and several values of K. In both figures the curves drawn for Rayleigh fading approach the respective non-fading related curves as K increases. It is noted that due to the numerically instability of (1.15) Monte-Carlo simulation is used to produce the curves.

Next, the analysis of the ICTS protocol is considered, according to which in the linear Wyner model, odd and even cells are active alternatively in orthogonal channels. Hence, inter-cell interference is avoided (thus, it is clearly non-interference limited). Starting with the non-fading setup the achievable sum-rate is easily shown to be

$$R_{\text{icts}} = \frac{1}{2}\log(1 + 2\bar{P}) \ , \tag{1.17}$$

where the pre-log factor of 1/2 and the power factor of 2 comes from the fact that each cell users transmit only half the time using twice the available average power. It is noted that this rate is achieved (not uniquely) by intra-cell TDMA and WB schemes. Deploying a similar protocol for the planar model where each cell is active only 1/6 of the time using $6\bar{P}$ power result in

$$\hat{R}_{\text{icts}} = \frac{1}{6}\log(1 + 6\bar{P}) \ . \tag{1.18}$$

Comparing the rate (1.9) with the performance of ICTS (1.17) for the linear model reveals that $R_{\text{icts}} > R_{\text{scp}}$ if the average power (or total cell SNR) $\bar{P}$ is above a certain threshold which is given by

$$\bar{P}_{\text{th}}(\alpha) = \frac{1 - 4\alpha^2}{8\alpha^4} \ . \tag{1.19}$$

It is observed that that for $\alpha > 1/2$, $R_{\text{icts}} > R_{\text{scp}}$ for any value of $\bar{P}$.

The extreme SNR analysis of ICTS in a non-fading scenario leads to

$$\begin{array}{llll} S_0 = 1 \ ; & \frac{E_b}{N_0\,\min} = \log 2 \ ; & S_\infty = \frac{1}{2} \ ; & \mathcal{L}_\infty = -1 \\ \hat{S}_0 = \frac{1}{3} \ ; & \frac{\hat{E}_b}{N_0\,\min} = \log 2 \ ; & \hat{S}_\infty = \frac{1}{6} \ ; & \hat{\mathcal{L}}_\infty = -(1 + \log_2 3) \ , \end{array} \tag{1.20}$$

proving that, as expected, ICTS is not interference-limited.

Introducing flat fading it is easily verified that the rate of the linear model is given by

$$R^*_{\text{icts}} = \frac{1}{2}E\left\{\log\left(1+\frac{2\bar{P}}{K}\sum_{k=1}^{K}|a_k|^2\right)\right\} = \frac{1}{2}E\left\{\log\left(1+\frac{\bar{P}}{K}S\right)\right\}, \tag{1.21}$$

where the rate for the intra-cell TDMA is achieved by setting $K=1$. For the special case of Rayleigh fading where $S = 2\sum_{k=1}^{K}|a_k|^2$ is distributed as $S \sim \chi^2_{2K}$ the rate is shown in [15] to be given by

$$R^*_{\text{icts}} = \frac{(-1)^K}{2\Gamma(K)}\frac{\partial^{K-1}}{\partial\mu^{K-1}}\left[\frac{-1}{\mu}\exp\left(\frac{K\mu}{2\bar{P}}\right)\text{Ei}\left(\frac{K\mu}{2\bar{P}}\right)\right]_{\mu=1}, \tag{1.22}$$

where $\text{Ei}(\cdot)$ is the exponential integral function. It is noted that the rate of the planar model is achieved by dividing (1.22) by 3 and replacing $\bar{P}$ with $3\bar{P}$.

Applying the Jensen's inequality to (1.21), it is easily verified that the presence of fading decreases the sum-rate $R^*_{\text{icts}} \leq R_{\text{icts}}$. Furthermore, increasing the number of users while keeping $\bar{P}$ constant, and applying the SLLN to (1.21), the rate boils down to (1.17). Hence, as already discussed above, the effect of fading is vanishing for the WB protocol with increasing K. Finally, applying the Jensen's inequality to (1.21) in a reverse manner reveals that for the ICTS protocol the WB scheme outperforms the intra-cell TDMA scheme in the presence of fading. It is noted that the results mentioned in this paragraph are valid for a general zero mean fading distribution with unit power and also for the planar model.

In the extreme SNR scenarios, and in presence of Rayleigh fading, characterization of the performance of ICTS reads

$$\begin{array}{lllll} S_0^* = \frac{1}{1+\frac{1}{2K}}\ ; & \frac{E_b}{N_0}^*_{\min} = \log 2\ ; & S_\infty^* = \frac{1}{2}\ ; & \mathcal{L}_\infty^* = \log_2 K + \left(\gamma - \sum_{\ell=1}^{K-1}\frac{1}{\ell}\right)\log_2 e - 1 \\ \hat{S}_0^* = \frac{1}{3(1+\frac{1}{2K})}\ ; & \frac{\hat{E}_b}{N_0}^*_{\min} = \log 2\ ; & \hat{S}_\infty^* = \frac{1}{6}\ ; & \hat{\mathcal{L}}_\infty^* = \log_2 K + \left(\gamma - \sum_{\ell=1}^{K-1}\frac{1}{\ell}\right)\log_2 e - 1 - \log_2 3\ , \end{array} \tag{1.23}$$

where γ is the Euler-Mascheroni constant

$$\gamma = \lim_{n\to\infty}\left(\sum_{\ell=1}^{n}\frac{1}{\ell} - \log n\right) \approx 0.5772\ . \tag{1.24}$$

As discussed above, parameters (1.23) coincides with the ones of a Gaussian scenario (1.20) asymptotically with increasing number of users K.

In Fig. 1.3 the non-interference limited behavior of the linear model ICTS spectral efficiency is demonstrated for $\alpha = 0.4$ and several values of K. The superiority of the ICTS over SCP for a fixed transmission power and increasing interference power is demonstrated in Fig. 1.4 for $\bar{P} = 10$ [dB] and several values of K. In both figures the curves drawn for Rayleigh fading approach the respective non-fading related curves as K increases. As with SCP protocol, Monte-Carlo simulation is used to produce the curves.

The reader is referred to [15] for a comprehensive study of single cell processing in the uplink of Wyner's linear and planar models.

1.3.2 Multi-Cell Processing

In this section joint processing of all signals received by all cell-sites is considered. As mentioned earlier, the central receiver is aware of all the users' codebooks and CSI, and the users are not allowed to cooperate. Accounting for the underlying assumptions, the overall channel is a Gaussian MAC with KM single antenna users and M distributed antenna receiver. Assuming an optimal decoding the per-cell sum-rate capacity of the linear model is given by

$$\begin{aligned} C^{*}_{\text{mcp}} &= \frac{1}{M} E\left\{ \log\det\left(\boldsymbol{I} + \frac{\bar{P}}{K} \boldsymbol{H}\boldsymbol{H}^{\dagger} \right) \right\} \\ &= E\left\{ \frac{1}{M} \sum_{m=1}^{M} \log(1 + \frac{\bar{P}}{K} \lambda_m(\boldsymbol{H}\boldsymbol{H}^{\dagger})) \right\} \\ &= E\left\{ \int_0^{\infty} \log\left(1 + \frac{\bar{P}}{K} x\right) dF^{M}_{\boldsymbol{H}\boldsymbol{H}^{\dagger}}(x) \right\} \end{aligned} \tag{1.25}$$

where $\boldsymbol{H}$ is the channel transfer matrix defined in (1.8), $\{\lambda_m(\boldsymbol{H}\boldsymbol{H}^{\dagger})\}_{m=1}^{M}$ are the non-negative eigenvalues of the semi-positive definite (SPD) matrix $\boldsymbol{H}\boldsymbol{H}^{\dagger}$, and $F^{M}_{\boldsymbol{H}\boldsymbol{H}^{\dagger}}(x)$ denotes

the empirical cumulative distribution function (or *spectrum*) of $\{\lambda_m(\boldsymbol{H}\boldsymbol{H}^\dagger)\}_{m=1}^M$, defined as

$$F^M_{\boldsymbol{H}\boldsymbol{H}^\dagger}(x) = \frac{1}{M}\sum_{m=1}^{M} 1_{\{\lambda_m(\boldsymbol{H}\boldsymbol{H}^\dagger)\leq\ x\}}, \tag{1.26}$$

and $1_{\{\cdot\}}$ is the indicator function. The spectrum of the eigenvalues of $\boldsymbol{H}\boldsymbol{H}^\dagger$ plays a key role in the sum-rate capacity calculation. Unfortunately, the power profile of $\boldsymbol{H}$ for finite K does not converge uniformly as the matrix dimensions increase [4]. Hence, *Girko*'s law for the eigenvalues of large random matrices cannot be applied to evaluate the sum-rate of (1.25) [4].

The system topology, according to which interferences arises only from adjacent cells, is well reflected in the five diagonal structure of $\boldsymbol{H}\boldsymbol{H}^\dagger$ which is explicitly given by

$$\left[\boldsymbol{H}\boldsymbol{H}^\dagger\right]_{(m,n)} = \begin{cases} \sum_{k=1}^{K}\left(|a_k^n|^2 + \alpha^2\,|b_k^n|^2 + \alpha^2\,|c_k^n|^2\right) & (n,n) \\ \alpha\sum_{k=1}^{K}\left(a_k^n(b_k^{n+1})^\dagger + c_k^n(a_k^{n+1})^\dagger\right) & (n,n+1) \\ \alpha\sum_{k=1}^{K}\left(a_k^n(c_k^{n-1})^\dagger + b_k^n(a_k^{n-1})^\dagger\right) & (n,n-1) \\ \alpha^2\sum_{k=1}^{K} c_k^n(b_k^{n+2})^\dagger & (n,n+2) \\ \alpha^2\sum_{k=1}^{K} b_k^n(c_k^{n-2})^\dagger & (n,n-2) \\ 0 & \text{otherwise} \end{cases}, \tag{1.27}$$

where out-of-range indices should be ignored.

The rest of this section is dedicated to the evaluation of (1.25) under various conditions. Starting with the non-fading setup, already treated by Wyner in [6], it is easily verified that $\frac{1}{K}\boldsymbol{H}\boldsymbol{H}^\dagger$ becomes a five diagonal Toeplitz matrix

$$\frac{1}{K}\left[\boldsymbol{H}\boldsymbol{H}^\dagger\right]_{(m,n)} = \begin{cases} (1+2\alpha^2) & (n,n) \\ 2\alpha & (n,n\pm1) \\ \alpha^2 & (n,n\pm2) \\ 0 & \text{otherwise} \end{cases}. \tag{1.28}$$

Applying *Szego*'s Theorem regarding the limit spectrum of infinite Toeplitz matrices [16],

the per-cell sum-rate capacity for the infinite linear array is given by

$$R_{\text{mcp}} \underset{M\to\infty}{=} \int_0^1 \log\left\{1+\bar{P}\left(1+2\alpha\cos(2\pi\theta)\right)^2\right\} d\theta \ . \tag{1.29}$$

Since the entries of $\frac{1}{K}\boldsymbol{H}\boldsymbol{H}^{\dagger}$ are independent of K for a fixed $\bar{P}$, this rate is achievable (not uniquely) by intra-cell TDMA and WB protocols. Applying the two dimensional version of *Szego*'s theorem the sum-rate capacity of the planar model is given by

$$\hat{R}_{\text{mcp}} \underset{M\to\infty}{=} \int_0^1\int_0^1 \log\left\{1+\bar{P}\left(1+2\alpha F(\theta_1,\theta_2)\right)^2\right\} d\theta_1 d\theta_2 \ , \tag{1.30}$$

where

$$F(\theta_1,\theta_2) \triangleq \cos(2\pi\theta_1)+\cos(2\pi\theta_2)+\cos\left(2\pi(\theta_1+\theta_2)\right) \ . \tag{1.31}$$

Extreme SNR characterization of MCP over Gaussian channels is summarized for the linear and planar models for $M\to\infty$, as follows

$$\begin{array}{cc}
S_0 = \frac{2(1+2\alpha^2)^2}{1+12\alpha^2+6\alpha^4} \ ; & \frac{E_b}{N_0\,\min} = \frac{\log 2}{1+2\alpha^2} \\
S_\infty = 1 \ ; & \mathcal{L}_\infty = \begin{cases} -2\log_2\left(\frac{1+\sqrt{1-4\alpha^2}}{2}\right) & 0\le\alpha\le\frac{1}{2} \\ -2\log_2\alpha & \alpha>\frac{1}{2} \end{cases} \\
\hat{S}_0 = \frac{2(1+6\alpha^2)^2}{1+36\alpha^2+48\alpha^3+90\alpha^4} \ ; & \frac{\hat{E}_b}{N_0\,\min} = \frac{\log 2}{1+6\alpha^2} \\
\hat{S}_\infty = 1 \ ; & \hat{\mathcal{L}}_\infty = -2\int_0^1\int_0^1 \log_2\left|1+2\alpha F(\theta_1,\theta_2)\right| d\theta_1 d\theta_2 .
\end{array} \tag{1.32}$$

Examining the power offset of the linear model, it is concluded that in the high-SNR regime and in the absence of fading, high inter-cell interference ($\alpha\approx 1$) or low inter-cell interference ($\alpha\approx 0$) are favorable, while intermediate inter-cell interference ($\alpha\approx 1/2$) provides the worse case scenario in terms of the spectral efficiency. This conclusion is well demonstrated in Fig. 1.4 already for $\bar{P}=10$ [dB]. Numerical calculations (not presented here) show that for $\bar{P}<1$ (or 0 [dB]), the sum-rate increases with α. Since the MCP is the capacity achieving strategy it rates are superior to both SCP and ICTS protocols under any condition, as is demonstrated in Figures 1.3 and 1.4.

The analysis of the fading case for finite K, is impaired by the fact that the spectrum of the resulting finite band matrix $\boldsymbol{H}\boldsymbol{H}^{\dagger}$ is currently not known even for increasing matrix dimensions $M \to \infty$. Therefore, techniques such as bounding, asymptotics, and extreme-SNR analysis, are used in order to get further insight into the performance merits of interest. These alternatives are explored below. Nevertheless, a simple observation can be achieved by applying the Jensen's inequality in a reverse manner to the first equality of (1.25). Accordingly it is concluded that in the presence of fading the MCP WB protocol ($K > 1$) outperforms the MCP intra-cell TDMA protocol ($K = 1$) [17]. This observation is demonstrated for Rayleigh fading in Figures 1.3 and 1.4 where the curves of the MCB WB protocol surpass the the curves of the MCP intra-cell TDMA protocol. It is noted that both curves are produced by Mote-Carlo simulations of a system with $M = 40$ cells.

Moments bounds

Turning to the flat fading setup it is easily verified that the n-th moment of the spectrum of $\boldsymbol{H}\boldsymbol{H}^{\dagger}$ is given by

$$\mathcal{M}_n = \lim_{M\to\infty} \frac{1}{M} \operatorname{tr}\left\{(\boldsymbol{H}\boldsymbol{H}^{\dagger})^n\right\} , \tag{1.33}$$

where the matrices multiplication $(\boldsymbol{H}\boldsymbol{H}^{\dagger})^n$ may be interpreted as paths weight summation over a restricted grid (see [17] for more details). In the special case where the amplitude of an individual fading coefficient is statistically independent of its uniformly distributed phase (e.g. *Rayleigh* fading) and intra-cell TDMA protocol is deployed ($K = 1$), a symbolic mathematics software has been reported in [17] to obtain the limit moments. For example, listed below are the first three limit moments:

$$\begin{aligned}
\mathcal{M}_1 &= m_2 + 2m_2\alpha^2 \\
\mathcal{M}_2 &= m_4 + 8m_2^2\alpha^2 + (4m_2^2 + 2m_4)\alpha^4 \\
\mathcal{M}_3 &= m_6 + (6m_2^3 + 12m_2m_4)\alpha^2 + (36m_2^3 + 12m_2m_4)\alpha^4 + (6m_2^3 + 12m_2m_4 + 2m_6)\alpha^6 ,
\end{aligned} \tag{1.34}$$

where m_i is the i-th moments of the amplitude of an individual fading coefficient. In case the limit moments do not grow too fast $\sqrt[2n]{\mathcal{M}_{2n}} = O(n)$ then according to Theorem (3.12) of [18], the spectrum of (1.26) converges weakly to a *unique* limit spectrum (defined by the

limit moments)

$$F^{M}_{\boldsymbol{HH}^{\dagger}}(x) \underset{M\to\infty}{\overset{\mathrm{d}}{\to}} F_{\boldsymbol{HH}^{\dagger}}(x) \ . \tag{1.35}$$

It is noted that Rayleigh fading satisfies this last condition. Identifying that the triplex, $\{\log(1+\bar{P}x),\ \{x^l\}_{l=1}^{n},\ F_{\boldsymbol{HH}^{\dagger}}(x)\}$, forms a T_{+}^{0} *Tchebychev* system, then the upper and lower principle representations (see [19]) of $F_{\boldsymbol{HH}^{\dagger}}(x)$ can be used to produced analytical lower and upper bound to the per-cell sum-rate capacity. For example, listed below are the lower and upper bounds of order $n = 2$ derived by this method

$$\frac{(\mathcal{M}_1)^2}{\mathcal{M}_2}\log\left(1+\bar{P}\frac{\mathcal{M}_2}{\mathcal{M}_1}\right) \le R^{*}_{\mathrm{msp}} \le \log\left(1+\bar{P}\mathcal{M}_1\right) \ , \tag{1.36}$$

where $\mathcal{M}_1$ and $\mathcal{M}_2$ are the first and second limit moments of $F_{\boldsymbol{HH}^{\dagger}}(x)$ given in (1.34). It is noted that applying *Jensen's* inequality to the first equality of (1.25) yields the upper bound of (1.36). For higher orders (higher values of n), it is necessary to use a symbolic mathematics software in order to find the probability masses of the upper and lower principal representation and their locations [17]. Examining the moment bounds (orders $n = 8,\ 10$) calculated for Rayleigh fading and presented in Fig. 1.4, reveal that the bounds are uniform in the interference factor α and get tighter as the order n increases. Additional calculations [17] (not presented here) show that the bounds are tighter when $\bar{P}$ decreases. In addition, in contrast to the SCP and ICTS protocols, the rate of MCP intra-cell TDMA ($K = 1$) increases in the presence of Rayleigh fading for certain values of α and $\bar{P}$. It is noted that the moments bounding technique is applicable (although in a tedious manner) for any finite K and also for the planar model.

Asymptotes with the number of users K

Focusing on the case where the number of users is large while $\bar{P}$ is kept constant, and applying the SLLN, the entries of $\frac{1}{K}\boldsymbol{H}\boldsymbol{H}^{\dagger}$ consolidate almost surely to their mean values

$$\frac{1}{K}\left[\boldsymbol{H}\boldsymbol{H}^{\dagger}\right]_{(m,n)} \overset{\text{a.s.}}{\underset{K\to\infty}{\longrightarrow}} \begin{cases} 1+2\alpha^2 & (n,n) \\ 2\alpha(1-\sigma_a^2) & (n,n\pm 1) \\ \alpha^2(1-\sigma_a^2) & (n,n\pm 2) \\ 0 & \text{otherwise} \end{cases}, \tag{1.37}$$

where $0 \leq \sigma_a^2 \leq 1$ is the variance of an individual unit gain fading coefficient. Hence, in the limit where K is large $\frac{1}{K}\boldsymbol{H}\boldsymbol{H}^{\dagger}$ becomes Toeplitz and by applying Szego's Theorem, the per-cell sum-rate capacity of the infinite linear model is approximated by

$$R^{*}_{\text{msp}} \underset{M,K\to\infty}{=} \int_0^1 \log\left\{1+\bar{P}\left[\sigma_a^2(1+2\alpha^2)+(1-\sigma_a^2)\left(1+2\alpha\cos(2\pi\theta)\right)^2\right]\right\} d\theta \ . \tag{1.38}$$

Adhering to similar argumentation and applying the two-dimensional Szego's theorem, the per-cell sum-rate capacity of the infinite planar model is approximated by

$$\hat{R}^{*}_{\text{mcp}} \underset{M,K\to\infty}{=} \int_0^1\int_0^1 \log\left\{1+\bar{P}\left[\sigma_a^2(1+6\alpha^2)+(1-\sigma_a^2)\left(1+2\alpha F(\theta_1,\theta_2)\right)^2\right]\right\} d\theta_1 d\theta_2 \ . \tag{1.39}$$

Since the same results, derived for a general fading distribution, are achieved by applying the Jensen's inequality to (1.25) it is concluded that the asymptotic expressions upper bound the sum-rates achieved for any finite number of users K. Another observation is made by noting that both expressions *increase* with σ_a^2 [17]; it is concluded that for MCP WB protocol and large number of users per cell $K \gg 1$, the presence of fading is beneficial under any condition. This performance enhancement is due to the independence of the three fading processes affecting the signal of each user, as observed by the three receiving cell sites, which explains why mimicking artificial fading at the users' transmitters fails to produce the same impact [17]. The sum-rates (1.38) and (1.39) are maximized for $\sigma_a^2 = 1$ which is corresponding to a zero-mean unit gain fading distribution (e.g. Rayleigh fading) and is

given by

$$R^*_{\text{msp}} \underset{\substack{M,K\to\infty \\ \sigma_a^2=1}}{=} \log\left(1+(1+2\alpha^2)\bar{P}\right) \ , \tag{1.40}$$

for the infinite linear model, and by

$$\hat{R}^*_{\text{msp}} \underset{\substack{M,K\to\infty \\ \sigma_a^2=1}}{=} \log\left(1+(1+6\alpha^2)\bar{P}\right) \ , \tag{1.41}$$

for the planar model. Examining (1.40) a *resource pooling* effect is revealed, as the rate coincides with a rate of an equivalent single-user non-fading link but with channel gain of $(1+2\alpha^2)$. The latter gain reflects the array power gain of the linear system ($(1+6\alpha^2)$ for the planar model).

Figures 1.3 and 1.4 demonstrate the tightness of the asymptotic expression (and upper bound) (1.40) already for a moderate number of users K. The fact that the presence of fading is beneficial for the MCP WB protocol with large K for all values of $\bar{P}$ and α is also demonstrated in Figures 1.3 and 1.4 where the asymptotic curves surpasses the no-fading corresponding curves.

Extreme SNR analysis

Extreme SNR characterization of the MCP protocol per-cell sum-rate is summarized for the linear model in the presence of Rayleigh fading and $M\to\infty$, as follows

$$S_0^* = \tfrac{2K}{1+K} \ ; \ \ \tfrac{E_b}{N_0}^*_{\min} = \tfrac{\log 2}{1+2\alpha^2} \ ; \ \ \tfrac{1}{2} \le S_\infty^* \le 1 \ ; -1-\log_2(1+2\alpha^2) \le \mathcal{L}_\infty^* \le -\log_2(1+2\alpha^2) \ . \tag{1.42}$$

Surprisingly, the low-SNR slope S_0^* is independent of α which comes in contrast to the low-SNR slope of the corresponding non-fading setup (1.54). Comparing the parameters of the MCP for the fading and non-fading linear setups (given in (1.42) and (1.54) respectively), reveals that the in the low-SNR regime the presence of Rayleigh fading is already beneficial

for K values above a threshold given by

$$K_t(\alpha) = \left\lceil \frac{(1+2\alpha^2)^2}{2\alpha^2(4+\alpha^2)} \right\rceil \ , \tag{1.43}$$

which is a decreasing function of α. Accordingly, in the low-SNR regime the presence of Rayleigh fading is beneficial for the MCP intra-cell TDMA protocol ($K = 1$), for $\alpha \gtrsim 0.54$. It is noted that the bounds in (1.42) for the high-SNR regime parameters are derived by the fact that the MCP WB protocol sum-rate increases with K in the presence of fading and is upper bounded for $K \to \infty$ by (1.40). Hence, the second order moment bound (derived for $K = 1$) (1.36) and (1.40) are a lower and an upper bound on the sum-rate respectively. However, a closed form expressions for the MCP protocol high-SNR parameters in the presence of fading for finite K, is still an open problem.

1.4 The Downlink Channel

Collecting the baseband signals received by all the terminals in the system at a given time instant in a $MK \times 1$ vector $\boldsymbol{y}$, the input-output equation for the downlink of the linear Wyner model with M cells, reads

$$\boldsymbol{y} = \boldsymbol{H}^{\dagger}\boldsymbol{x} + \boldsymbol{z} \ . \tag{1.44}$$

where the channel transfer matrix $\boldsymbol{H}$ is defined as in (1.7), with $\boldsymbol{a}_m$, $\boldsymbol{b}_m$ and $\boldsymbol{c}_m$ here defining the $1 \times K$ row vectors denoting the channel complex fading coefficients, experienced by the K users of the m-th, $(m-1)$-th, and $(m+1)$-th cells, respectively, when receiving the transmissions of the m-th cell-site antenna. Full CSI is assumed available to the joint multi-cell transmitter. The latter assumption implies the availability of a feedback channel from the users to the APs. On the other hand, the mobile receivers are assumed to be cognizant of their own CSI, and of the employed transmission strategy. In addition, $\boldsymbol{x}$ is the $M \times 1$ complex Gaussian vector of signals transmitted by the M cell-sites $\boldsymbol{x} \sim \mathcal{CN}(0, \boldsymbol{P})$. As explained in Sec. 1.2, an *equal individual per-cell power constraint* of $[\boldsymbol{P}]_{(m,m)} \leq \bar{P}\ \forall m$ is assumed. Lastly, $\boldsymbol{z}$ is the $MK \times 1$ complex Gaussian additive noise vector $\boldsymbol{z} \sim \mathcal{CN}(0, \boldsymbol{I}_{MK})$.

1.4.1 Single-Cell Processing

Starting with the Gaussian case, the per cell sum-rates for the linear and planar models are equal to the respective uplink rates, (1.9) and (1.10). In the presence of Rayleigh fading, and assuming each cell-site is aware of its users' instantaneous channel gain and instantaneous interference power, a suboptimal scheme that schedules the "best" user for transmission in each cell, is considered. The following rate is achieved for the linear model:

$$R^*_{\text{scp}} = E\left\{\log\left(1+\max_k \text{SNR}_k\right)\right\}, \tag{1.45}$$

where the i.i.d random variable SNRs are given by

$$\text{SNR}_k = \frac{\bar{P}\,|a_k|^2}{1+\alpha^2\bar{P}(|b_k|^2+|c_k|^2)}\ . \tag{1.46}$$

Following [14] the probability density function (PDF) and cumulative distribution function (CDF) of an arbitrary SNR_k (1.46) are given by

$$f_s(x) = \frac{\alpha^2 e^{-x/\bar{P}}}{(1+\alpha^2 x)^3}\left(\frac{1}{\alpha^2\bar{P}}(1+\alpha^2 x)+2\right) \quad ; \quad x\geq 0\ , \tag{1.47}$$

and

$$F_s(x) = 1-\frac{e^{-x/\bar{P}}}{(1+\alpha^2 x)^2} \quad ; \quad x\geq 0\ . \tag{1.48}$$

Since $\max_k \text{SNR}_k$ is distributed according to $f_{\tilde{s}}(x) = K f_s(x)(F_s(x))^{K-1}$ the sum-rate (1.45) is given by

$$R^*_{\text{scp}} = K\int_0^\infty \log(1+x)\left(1-\frac{e^{-x/\bar{P}}}{(1+\alpha^2 x)^2}\right)^{K-1}\frac{\alpha^2 e^{-x/\bar{P}}}{(1+\alpha^2 x)^3}\left(\frac{1}{\alpha^2\bar{P}}(1+\alpha^2 x)+2\right)dx\ . \tag{1.49}$$

Adhering to similar argumentation, the sum-rate for the planar model is given by

$$\hat{R}^*_{\text{scp}} = K\int_0^\infty \log(1+x)\left(1-\frac{e^{-x/\bar{P}}}{(1+\alpha^2 x)^4}\right)^{K-1}\frac{\alpha^2 e^{-x/\bar{P}}}{(1+\alpha^2 x)^5}\left(\frac{1}{\alpha^2\bar{P}}(1+\alpha^2 x)+4\right)dx\ . \tag{1.50}$$

For increasing number of users K and fixed $\bar{P}$, the maximum SNR in the linear and planar models, behaves with high probability like $\bar{P}\log K + O(\log\log K)$ [14]. Hence, for fixed $\bar{P}$, the SCP sum-rate of both models behaves like

$$R^*_{\text{scp}} = \hat{R}^*_{\text{scp}} \underset{K\gg 1}{\cong} \log(1+\bar{P}\log K)\ , \tag{1.51}$$

and a scaling law of $\log\log K$ with increasing number of users per-cell is revealed. On the other hand, for any finite K, the rates demonstrates an interference limited behavior. Hence, $S^*_\infty = \hat{S}^*_\infty = 0$. The interference limited behavior of the SCP protocol (linear model) in the presence of Rayleigh fading is demonstrated in Fig. 1.5 using Monte-Carlo simulations for $K = 100$ users and $\alpha = 0.4$.

As with the SCP protocol, the per cell sum-rates of the ICTS protocol for the linear and planar models are equal to the respective uplink rates, (1.17) and (1.18). In the presence of Rayleigh fading the following sum-rate is achieved by scheduling the "best" user for transmission [20]

$$R^*_{\text{icts}} = \frac{K}{2}\int_0^\infty \log(1+2\bar{P}x)e^{-x}\left(1-e^{-x}\right)^{K-1}dx\ . \tag{1.52}$$

Since $\max\limits_{1\le k\le K}|a_k|^2$ (where $|a_k|^2 \sim \chi^2_2\ \forall k$ and i.i.d.), behaves with high probability like $\log K + O(\log\log K)$ for $K \gg 1$ [14], (1.52) is well approximated for a large number of users per cell, by

$$R^*_{\text{icts}} \underset{K\gg 1}{\cong} \frac{1}{2}\log(1+2\bar{P}\log K)\ . \tag{1.53}$$

The respective rates for the planar model are obtained by replacing the constant 2 by 6, which reflects the fact that each cell is active 1/6 of the time. It is concluded that for fixed $\bar{P}$ the ICTS per-cell sum-rates of the linear and planar models scale as $\frac{1}{2}\log\log K$ and $\frac{1}{6}\log\log K$ respectively. The high-SNR regime of the ICTS protocol sum-rate per-cell is characterized for large K by

$$\begin{aligned} S^*_\infty &= \tfrac{1}{2}\ ; \qquad \mathcal{L}_\infty = -\log_2\log K - 1 \\ \hat{S}^*_\infty &= \tfrac{1}{6}\ ; \quad \hat{\mathcal{L}}_\infty = -\log_2\log K - 1 - \log_2 3\ . \end{aligned} \tag{1.54}$$

The inherent non-interference behavior and high-SNR slope of the ICTS protocol are demonstrated in the presence of Rayleigh fading in Fig. 1.5 using Monte-Carlo simulations for $K = 100$ and $\alpha = 0.4$. The inferior scaling law of the ICTS protocol in comparison to the SCP protocol (linear model) is demonstrated in Fig. 1.6, using Monte-carlo simulations for $\alpha = 0.4$ and $\bar{P} = 10$ [dB].

1.4.2 Multi-Cell Processing

The key tool used in the analysis to follow is a recent result by Yu and Lan [21], who established a connection between the uplink-downlink duality of the Gaussian vector MAC and BC, and the Lagrangian duality in minimax optimization. Accordingly, the sum-rate capacity of the Wyner's downlink channel with per-cell power constraint, equals the sum-rate capacity of its dual uplink channel, subject to an overall sum power constraint determining the level of cooperation between the users, and a noise power constraint capturing the equal per-cell power constraints of the original downlink channel. Hence, the per-cell sum-rate capacity of the downlink channel is given by

$$R^*_{\text{msp}} = \frac{1}{M} E_H \left\{ \min_{\boldsymbol{\Lambda}} \max_{\boldsymbol{D}} \log \frac{\det\left(\boldsymbol{H}\boldsymbol{D}\boldsymbol{H}^\dagger + \boldsymbol{\Lambda}\right)}{\det\left(\boldsymbol{\Lambda}\right)} \right\}, \tag{1.55}$$

where the optimization is over all nonnegative $MK \times MK$ and $M \times M$ *diagonal* matrices, $\boldsymbol{D}$ and $\boldsymbol{\Lambda}$, satisfying $\text{tr}(\boldsymbol{D}) \leq M\bar{P}$ and $\text{tr}\left(\boldsymbol{\Lambda}\right) \leq M$, respectively.

This optimization problem was recently studied in [22] [23] for the *circular* Wyner model. For the non fading setup it is proved that the sum-rate (1.55), is equal to the sum-rate capacity of the uplink channel (1.29) [23]:

$$R_{\text{mcp}} \underset{M\to\infty}{=} \int_0^1 \log\left(1 + \bar{P}(1 + 2\alpha\cos(2\pi\theta))^2\right) d\theta. \tag{1.56}$$

This rate is achieved by *dirty paper coding* (DPC) techniques [3] [2]. In fact, the equivalence between the downlink and uplink channels is shown to hold for *any* circulant channel transfer matrix [23]. The proof of this results is based on the symmetry induced by the non-fading

circulant channel transfer matrix, and on a result by [24], according to which the inner term of (1.55) is convex in $\boldsymbol{\Lambda}$ and concave in $\boldsymbol{D}$ (for more details see [23]).

For Rayleigh flat fading channels, upper and lower (achievable rate) bounds are derived, while focusing on the asymptotic regime in terms of the number of users per cell. The achievable rate is obtained by employing a power control scheme in the *dual uplink channel*, according to which only users received at all three cell-sites with fade power levels exceeding some constant L are active. As $K \to \infty$ the number of active users per cell crystallizes to $K_0 \triangleq Ke^{-3L}$, and it is assumed that all active users transmit at equal powers $\bar{P}/K_0$. The constant L should be chosen so that $K_0 \to \infty$ as $K \to \infty$ (and thus the SLLN can be applied). In particular, for $K_0 = Ke^{-3L} = K^{\epsilon}$ the threshold is set to $L = \frac{1-\epsilon}{3}\log K$, where $0 < \epsilon < 1$. The resulting large K achievable rate can be shown to constitute an upper bound for *any finite* K. It is noted that the threshold-crossing scheduling scheme used in the virtual dual uplink channel is an analysis tool and has little in common with the actual DPC used to achieve the sum-rate capacity.

The capacity upper bound is derived by bounding the channel fades by the strongest fading gain (over all intra-cell users) received at each cell-site, and observing that the maximum of K i.i.d. χ_2^2 distributed random variables behaves like $\log K + O(\log\log K)$ for $K \gg 1$ [14]. Combining the two bounds it can be concluded that for $K \gg 1$ the downlink average per-cell sum-rate capacity satisfies

$$\log\left(1 + \frac{(1+2\alpha^2)}{3}\bar{P}\left((1-\epsilon)\log K + 3\right)\right) \leq R^*_{\text{mcp}} \leq \log\left(1 + (1+2\alpha^2)\bar{P}\log K\right), \quad (1.57)$$

for some $\epsilon \underset{K\to\infty}{\to} 0$. Examining (1.57), it is observed that in addition to a non-interference limited behavior, both bounds increase with α. Moreover, both bounds demonstrates multi-user diversity gain of $\log K$ and scale like $\log\log K$ as K increases. In addition, the upper bound predicts an array power gain of $(1+2\alpha^2)$ in addition to the multi-user diversity gain. It is noted that the gap between the two bounds converge to $\log 3 \approx 1$ [nat/channel use] as the number of users per-cell increases. Finally, the high-SNR regime characterization of

R^*_{mcp} for large K is summarized as follows

$$\begin{aligned} &S^*_\infty = 1 \\ &-\log_2(1+2\alpha^2) - \log_2\log K \le \mathcal{L}^*_\infty \le -\log_2(1+2\alpha^2) - \log_2\left((1-\epsilon)\log K + 3\right) + \log_2 3 \ . \end{aligned} \tag{1.58}$$

In comparison to the respective non-fading setup parameters of (1.54), the presence of Rayleigh fading does not change the high-SNR slope, but a multiuser diversity gain of $\log K$ is observed in the power offset.

It is noted that finding an exact expression for sum-rate capacity of the Wyner downlink channel is still an open problem.

1.4.3 Distributed Zero Forcing Beamforming

In the previous section, bounds on the ultimate sum-rate under per-cell power constraint have been presented. In this section, as a practical alternative to optimal DPC schemes, zero-forcing beamforming (ZFBF) with a simple scheduling is considered. It is noted that ZFBF is an attractive scheduling scheme since it demonstrates non-interference limited behavior and require single user coding-decoding scheme. In addition, with N transmit antennas and K users, the sum-rate achieved by ZFBF to a "semi-orthogonal" subset of at most N users, demonstrates the same scaling law as the sum-rate achieved by the optimal DPC scheme for increasing number of users [25].

Consider the circular Wyner's model where $M > 2$ cells with K users each, are arranged on a circle. Assuming an intra-cell TDMA scheme, according to which only one user is selected for transmission per-cell, the $M \times 1$ vector baseband representation of the signals received by the *selected* users is given for an arbitrary time index by

$$\boldsymbol{y} = \boldsymbol{H}^\dagger \boldsymbol{B}\boldsymbol{u} + \boldsymbol{z} \ , \tag{1.59}$$

where $\boldsymbol{u}$ is the $M \times 1$ complex Gaussian symbols vector $\boldsymbol{u} \sim \mathcal{CN}(\boldsymbol{0}, \boldsymbol{I}_M)$, $\boldsymbol{B}$ is the beam-

forming $M \times M$ matrix:

$$\boldsymbol{B} = \sqrt{\frac{MP}{\mathrm{tr}\left((\boldsymbol{H}\boldsymbol{H}^{\dagger})^{-1}\right)}} \left(\boldsymbol{H}^{\dagger}\right)^{-1} , \tag{1.60}$$

with $M\bar{P}$ being the overall average transmit power constraint, which is ensured by definition[2], and $\boldsymbol{z}$ is the $M \times 1$ complex Gaussian additive noise vector $\boldsymbol{z} \sim \mathcal{CN}(\boldsymbol{0}, \boldsymbol{I}_M)$. Substituting (1.60) into (1.59), the received signal vector reduces to

$$\boldsymbol{y} = \sqrt{\frac{M\bar{P}}{\mathrm{tr}\left((\boldsymbol{H}\boldsymbol{H}^{\dagger})^{-1}\right)}}\, \boldsymbol{u} + \boldsymbol{z}. \tag{1.61}$$

Since, (1.61) can be interpreted as a set of M identical independent parallel single user channels, its ergodic achievable sum-rate per-channel (or cell) is given by

$$R^{*}_{\mathrm{zfbf}} = E\left\{\log\left(1 + \frac{M\bar{P}}{\mathrm{tr}\left((\boldsymbol{H}\boldsymbol{H}^{\dagger})^{-1}\right)}\right)\right\}. \tag{1.62}$$

Although an oveall power constraint is assumed, a more natural choice for a cellular system is to maintain per-cell power constraints. Hence, we are interested in the transmitted power of an arbitrary cell, which is averaged over the TDMA time slot duration (many symbols) and is a function of the realization of $\boldsymbol{H}$,

$$\bar{P}_m = [\boldsymbol{B}\boldsymbol{B}^{\dagger}]_{m,m} = \frac{M\bar{P}\left[(\boldsymbol{H}\boldsymbol{H}^{\dagger})^{-1}\right]_{m,m}}{\mathrm{tr}\left((\boldsymbol{H}\boldsymbol{H}^{\dagger})^{-1}\right)} . \tag{1.63}$$

For non-fading channels, a round-robin scheduling is deployed and there is no need to feed back the channel coefficients. In addition, for each time slot, the channel transfer matrix becomes circulant with $(1,\ \alpha,\ 0,\ \ldots\ 0,\ \alpha)$ as first row. Applying Szego's Theorem regarding the spectrum of Toeplitz matrices [16], the average per-cell sum-rate of the ZFBF scheme is given for $\alpha < 1/2$, by

$$R_{\mathrm{zfbf}} \underset{M\to\infty}{=} \log\left(1 + \mathcal{F}(\alpha)\ \bar{P}\right) , \tag{1.64}$$

[2]Later on it is argued that under certain conditions this scheme satisfies a per-cell average power constraints as well

where

$$\mathcal{F}(\alpha) \triangleq \frac{1}{\int_0^1 \left(1+2\alpha\cos(2\pi\theta)\right)^{-2} d\theta} \ . \tag{1.65}$$

This rate holds for an overall power constraint $M\bar{P}$, and for an *equal per-cell power constraints* $\bar{P}$. It is easily verified that $0 < \mathcal{F}(\alpha) \leq 1$ and that it is a decreasing function of the interference factor α. Comparing (1.64) to (1.17), it is clear that the ZFBF scheme is superior to the ICTS scheme when the SNR $\bar{P}$ is above a certain threshold

$$\bar{P}_{\rm t}(\alpha) = \frac{2(1-\mathcal{F}(\alpha))}{(\mathcal{F}(\alpha))^2} \ , \tag{1.66}$$

which is an increasing function of α. It is noted that for $\alpha = 1/2$ the circulant channel transfer matrix $\boldsymbol{H}$ is singular and channel inversion methods such as ZFBF are not applicable. Moreover, $\boldsymbol{H}$ is not guaranteed to be non-singular for $\alpha > 1/2$ and any finite number of cells M. The extreme SNR characterization of the ZFBF scheme is summarized by

$$S_0 = 2 \ ; \quad \tfrac{E_b}{N_0\,\min} = \tfrac{\log 2}{\mathcal{F}(\alpha)} \ ; \quad S_\infty = 1 \ ; \quad \mathcal{L}_\infty = -\log_2 \mathcal{F}(\alpha) \ , \tag{1.67}$$

proving a two fold rate gain in the high-SNR regime when compared to the ICTS protocol (1.20).

Turning to the Rayleigh fading setup, a simple scheduling algorithm that selects for each fading block (or TDMA slot) the user with the "best" local channel for transmission in each cell, is considered. In other words, the selected user in the m-th cell is

$$\tilde{k}(m) = \underset{k}{\rm argmax}\{|a_{m,k}|^2\} \ , \tag{1.68}$$

where $\{a_{m,k}\}_{k=1}^K$ are the fading coefficients of the m-th cell transmitted signals as they are received by the m-th cell users. The resulting channel transfer matrix $\boldsymbol{H}^\dagger$ of this sub-optimal scheduling, consists of diagonal entries $a_m = a_{m,\tilde{k}(m)}$ which their amplitudes are the *maximum* of K i.i.d. χ_2^2 distributed random variables. The other two diagonals entries of $\boldsymbol{H}^\dagger$ are χ_2^2 distributed random variables multiplied by α.

In case $\boldsymbol{H}$ is ill conditioned, the joint beamformer can start replacing the "best" users

by their second "best" users until the resulting $\boldsymbol{H}$ is well behaved. Since we assume that $K \gg 1$, the overall statistics is not expected to change by this users replacing procedure.

The special structure of the channel transfer matrix $\boldsymbol{H}^{\dagger}$ resulting from the setup topology and scheduling procedure, plays a key role in understanding the asymptotic scaling law of the scheme's per-cell sum-rate R^{*}_{zfbf} (expression (1.62)), which is asymptotically optimal with increasing number of users per-cell [26]:

$$\frac{R^{*}_{\text{zfbf}}}{R^{*}_{\text{msp}}} \underset{K\to\infty}{\longrightarrow} 1 \ . \tag{1.69}$$

where R^{*}_{msp}, which scales like $\log\log K$ is the per-cell sum-rate capacity of the channel and is bounded for large K in (1.57). This results, can be intuitively explained by the fact that due to the scheduling process, $(\boldsymbol{H}\boldsymbol{H}^{\dagger})$ "becomes" diagonal $(\log K \boldsymbol{I}_{M})$ when K increases. Accordingly, for large K, $(\boldsymbol{H}\boldsymbol{H}^{\dagger})^{-1}$ "behaves" like $(\boldsymbol{I}_{M}/\log K)$, and R^{*}_{zfbf} (expression (1.62)) is approximated by

$$R^{*}_{\text{zfbf}} \underset{K\gg 1}{\cong} \log(1+\bar{P}\log K) \ . \tag{1.70}$$

It is also concluded that the ZFBF scheme provides, a two fold scaling law than the per-cell sum-rate scaling law of the ICTS scheme (1.53), in the presence of Rayleigh fading. Moreover, by definition the sum-rate of the ZFBF scheme ensures a non-interference limited behavior for any number of users K (not necessarily large) in contrast to the rate achieved by the SCP protocol. The high-SNR characterization of the ZFBF scheme is summarized by

$$S^{*}_{\infty} = 1 \ ; \quad \mathcal{L}^{*}_{\infty} = -\log_2\log K \ , \tag{1.71}$$

Finally, the considered ZFBF scheme, that maintains an overall power constraint of $M\bar{P}$, is shown in [26] to ensure *in probability* an equal per-cell power constraint of $\bar{P}$, asymptotically with increasing number of users per-cell. Hence,

$$Pr\left(\bar{P}_{m} \leq \bar{P}+\epsilon\right) \underset{K\to\infty}{\longrightarrow} 1 \ , \tag{1.72}$$

for an arbitrary small $\epsilon > 0$. As mentioned earlier, for cellular systems an individual per-cell

power constraint is a more reasonable choice than a sum-power constraint which is more suitable for collocated antenna arrays.

In Fig. 1.5 the spectral efficiencies of the ZFBF scheme (Monte-Carlo simulation for $M = 40$), along with its asymptotic expression (1.70) and the sum-rate capacity upper bound (1.57), are plotted in the presence of Rayleigh fading for $K = 100$ and $\alpha = 0.4$. A good match between the asymptotic expression and the Monte-carlo simulation resulting curve is observed. It is noted that this match degrades for lower K or larger values of α (not presented here). The gap between the ZFBF curves and the sum-rate capacity upper bound is clearly explained by the fact that the ZFBF scheme does not use the antenna array to enhance the reception power but to eliminate inter-cell interferences. Hence, the additional array power gain of $(1 + 2\alpha^2)$ predicted by the upper bound can not be achieved. In addition, the performance gain of the ZFBF scheme over the SCP and ICTS protocols is clearly evident. In Fig. 1.6 the scaling law of the scheme with K is presented by Monte-Carlo simulations, and a good match to the asymptotic expression is observed. It is noted that the match degrades when the number of user decreases.

The reader is referred to [26] for more details on the analysis and derivations.

1.5 Cooperation Among Terminals

In this section, the benefits of cooperative transmission among terminals in a DAS is considered. A simple extension of the Wyner model that allows intra-cell terminal-to-terminal cooperation (recall Sec. 1.2.2) is analyzed in Sec. 1.5.1. Then, the per-cell throughput (sum-rate) of SCP and MCP with terminal cooperation is evaluated in Sec. 1.5.2 and 1.5.3 respectively, with special emphasis on the low-SNR regime.

1.5.1 Wyner's Model with Cooperation Among Terminals

The system layout is illustrated in Fig. 1.7. For simplicity, uplink channel and intra-cell TDMA scheme are considered. In each of the M cells, each active terminal has available a relay terminal for cooperation. As compared to the standard linear Wyner's model presented in Sec. 1.2.1, two new parameters β^2 and γ^2 are introduced that model the average channel gain power between the source terminal and its relay, and between relay and the corresponding AP, respectively. The channel gains relative to the signal received by APs of adjacent cells from source, terminal and relay equal the square of Wyner's inter-cell interference factor α^2. Notice that it is assumed that a relay receives with negligible power the signal transmitted by terminals belonging to adjacent cells. This assumption is reasonable if the relays are terminals, but it may be questionable if the relays are fixed wireless stations with antennas placed at heights comparable to the APs. Extension to a more general model can be easily derived from the treatment presented below, and it will not be further illustrated here for the sake of simplicity.

Cooperation between terminals is assumed to follow the decode and forward (DF) protocol, that is illustrated in Fig. 1.7 and discussed in [9]. In the first time-slot, each active terminal broadcasts to both its relay and AP. In the second time-slot, the relay forwards the decoded signal to the AP. Finally, the AP decodes by considering the signal received in both time-slots.

1.5.2 Single-Cell Processing and DF Cooperation Between Terminals

In this section, the scenario in Fig. 1.7 is investigated with SCP. According to the DF protocol, the codeword transmitted by the source terminal in the first slot must be decoded by the relay. Therefore, assuming that the relay is aware of the realization of the channel gain d_m (see Fig. 1.7), the achievable rate is limited by

$$R_{\text{scp+coop}} \leq R_{\text{relay}}(\bar{P}, \beta) = \frac{1}{2}\mathrm{E}_d\{\log\left(1 + \bar{P}\beta^2|d_m|^2\right)\}, \tag{1.73}$$

where the pre-log scaling factor 1/2 accounts for the two-slot transmission structure of DF. Moreover, conditioned on (1.73), the achievable rate at the AP, taking into account the signals received in both the first time-slot (directly from the source) and in the second (forwarded by the relay) is $R_{\text{scp+coop}} \leq R_{\text{d}}(\bar{P}, \alpha, \gamma)$, where [27]

$$R_{\text{d}}(\bar{P}, \alpha, \gamma) = \frac{1}{2}\text{E}\left\{\log\left(1 + \bar{P}\left[\begin{array}{cc} a_m^* & \gamma\tilde{a}_m^* \end{array}\right]\boldsymbol{Q}(\bar{P},\alpha)^{-1}\left[\begin{array}{c} a_m \\ \gamma\tilde{a}_m \end{array}\right]\right)\right\} , \tag{1.74}$$

with $\tilde{a}_m$ denoting the channel gain between relay and corresponding AP ($\tilde{b}_m$ and $\tilde{c}_m$ are similarly defined in accordance to the notation used throughout the chapter, see Fig. 1.7), and matrix $\mathbf{Q}(\bar{P},\alpha)$ accounting for correlation of the intercell interference in the two time-slots:

$$\boldsymbol{Q}(\bar{P},\alpha) = \left[\begin{array}{cc} 1 + \alpha^2\bar{P}(|b_m|^2 + |c_m|^2) & \alpha^2\bar{P}(b_m\tilde{b}_m^* + c_m\tilde{c}_m^*) \\ \alpha^2\bar{P}(b_m\tilde{b}_m^* + c_m\tilde{c}_m^*) & 1 + \alpha^2\bar{P}(|\tilde{b}_m|^2 + |\tilde{c}_m|^2) \end{array}\right] . \tag{1.75}$$

From (1.73) and (1.74), we finally get the ergodic per-cell achievable sum-rate:

$$R_{\text{scp+coop}} = \min\{R_{\text{relay}}(\bar{P}, \beta), R_{\text{d}}(\bar{P}, \alpha, \gamma)\} . \tag{1.76}$$

Low-SNR analysis

The low-SNR characterization of the achievable rate (1.76) can be shown as in [27] to read:

$$\frac{E_b}{N_{0\,\min}} = \max\left\{\frac{2\log 2}{\beta^2}, \frac{2\log 2}{1+\gamma^2}\right\} \quad ; \quad S_0 = \frac{1}{2}\min\left\{1, \frac{1 + 2\gamma^2 + \gamma^4}{2 + \gamma^2 + \gamma^4 + 6\alpha^2(1+\gamma^2)}\right\} . \tag{1.77}$$

In Fig. 1.8 the low-SNR approximation is compared with the exact throughput (1.76) for $\alpha^2 = -3$ [dB], $\beta^2 = 20$ [dB], and $\gamma^2 = 10$ [dB], showing that the approximation holds for spectral efficiencies as large as 0.4 [bit/sec/Hz]. From inspection of (1.77), it is clear that, if the average channel gains between relay and both active terminal and AP are larger than the average channel gain of the direct link between terminal and AP, or more precisely if $\beta^2 > 2$ and $\gamma^2 > 1$, then relevant gains in terms of minimum energy per bit can be obtained. On the other hand if $\beta^2 \leq 2$ or $\gamma^2 \leq 1$, cooperation between terminals yields a power loss as

compared to the non-cooperative case. On the other hand, the slope S_0 is at most 1/2 (for the example $S_0 = 0.4172$). This reduction in the low-SNR slope is immaterial if $E_b/N_{0\min}$ is sufficiently small as for the case in Fig. 1.8.

1.5.3 Multi-Cell Processing and DF Collaboration Between Terminals

In this section a multi-cell processing as in Sec. 1.3.2 is assumed. As explained above, the achievable rate, due to the DF protocol is limited by the maximum rate at which the relay is able to correctly decode the transmitted signal, i.e., $R_{\text{mcp+coop}} \leq R_{\text{relay}}(\bar{P}, \beta)$ (recall (1.73)). In the first time-slot, the signal received by the APs is (1.7) with $K = 1$, whereas in the second it has the same matricial formulation $\tilde{\boldsymbol{y}} = \tilde{\boldsymbol{H}}\boldsymbol{x} + \tilde{\boldsymbol{z}}$, but the channel matrix $\tilde{\boldsymbol{H}}$ contains the fading channels from the relays (see (1.8)). It follows that the achievable per-cell throughput satisfies the inequality $R_{\text{mcp+coop}} \leq R_{\text{m}}(\bar{P}, \alpha, \gamma)$:

$$R_{\text{m}}(\bar{P}, \alpha, \gamma) = \frac{1}{2M} E\{\log\det\{\boldsymbol{I} + \text{SNR}(\boldsymbol{H}\boldsymbol{H}^{\dagger} + \tilde{\boldsymbol{H}}\tilde{\boldsymbol{H}}^{\dagger})\}\} \ . \tag{1.78}$$

Then, similarly to (1.76),

$$R_{\text{mcp+coop}} = \min\{R_{\text{relay}}(\bar{P}, \beta), R_{\text{m}}(\bar{P}, \alpha, \gamma)\}. \tag{1.79}$$

Low-SNR analysis

The low-SNR characterization of multicell processing with DF cooperation between terminals reads for M large enough (see [27] for proof):

$$\begin{aligned} \frac{E_b}{N_0}_{\min} &= \max\left\{\frac{2\log 2}{\beta^2}, \frac{2\log 2}{1+\gamma^2+4\alpha^2}\right\} \\ S_0 &= \frac{1}{2}\min\left\{1, \frac{(1+4\alpha^2+\gamma^2)^2}{2(8\alpha^4+4\alpha^2(1+\gamma^2)+1+\gamma^4)}\right\} \ . \end{aligned} \tag{1.80}$$

Comparison between the actual throughput (1.79) and the affine low-SNR approximation is shown in Fig. 1.8 for $\alpha^2 = -3$ [dB], $\beta^2 = 20$ [dB], $\gamma^2 = 10$ [dB], and $M = 20$. From

(1.80) and (1.77), multi-cell processing proves to be beneficial in a system that employs DF cooperation at the terminals only if $\beta^2 > 1 + \gamma^2$ and in this case the energy gain is easily quantified as $\min\{(1+\gamma^2+4\alpha^2)/(1+\gamma^2), \beta^2/(1+\gamma^2)\}$ (equal to 0.72 [dB] in the example). It is noted that this problem could be alleviated by implementing the selective DF protocol proposed in [9], wherein if the channel gain between active terminal and relay falls between a given threshold then direct transmission is employed.

1.6 Perspectives and Discussion

The cell-sites antennas (or AP) of a cellular systems are spread over the coverage area of the network. At each time instance, the users "see" several co-located cell-sites. In conventional systems where each cell processes the signals of its own users treating other users as noise, this phenomenon leads to an interference-limited behavior that significantly affects the system performance. This problem is mitigated by sharing and reusing the degrees of freedom available to the network among the cells. On the other hand, by deploying joint processing of signals associated with the different APs, taking advantage of the powerful "backbone" network connecting the latter, the impact of interference can be theoretically eliminated, since interferences become useful signals. Moreover, spatial diversity and beamforming advantages can be harnessed as well to increase the overall system performance. In this Chapter, these principles are demonstrated for the family of Wyner cellular models, which lends itself to an analytical study, thus facilitating the insight in more involved and realistic settings.

Ending this Section is a brief list of open issues related to the information theoretic analysis of DAS under the Wyner model:

- derivation of a closed-form expression for the ergodic sum-rate of both uplink and downlink for finite number of users K: instrumental to this task is the calculation of the eigenvalues distribution of a finite band random matrix, which is to date an open problem even in the asymptotic case where the matrix dimensions are large;
- investigation of the effects of impairments (finite capacity, delay) on the backbone con-

necting APs: some preliminary results in this direction have been presented in [10] [11] and [8].

- analysis of the effects of reduced feedback (imperfect CSI) at the APs in the downlink: performance of suboptimal schemes that require a limited amount of feedback have been widely investigated in recent years for collocated antenna arrays in order to study the trade-off between multiuser diversity and feedback overhead. Extension to DAS within Wyner's model is a challenging task due to the unique structure of the problem;
- study of the benefits of cooperation among mobile terminals under general cooperative protocols, see, e.g., [9];
- the problem of optimal degrees of freedom allocation in the Wyner framework. As an example see the comprehensive discussion on ICTS protocols in [15].

1.7 Bibliographical Notes

The general framework of the "multi-receiver" network model was introduced and analyzed in [5] for Gaussian channels. The uplink channel of a simple cellular model referred to as the Wyner's linear and planar models are introduced and analyzed in [6] for optimal and linear MMSE MCP receivers, and Gaussian channels. It is noted that this model consists of a special case of the more general "multi-receiver" network model. [28] extends the Wyner model to include fading channels and analyzes the performance of single and two cell processing under various setups. In [17] the results of [6] are extended to include fading channels. [29] [30] consider SCP of randomly spread CDMA in Wyner's linear model for non-fading and flat fading respectively (see also [31]). [8] [7] extend the results of [29] [30] for MCP limiting the number of cooperating cells (clusters). Various iterative decoding schemes based on local message-passing between adjacent cells are considered in [32][11] [33][10][34] for the Wyner linear and planar models. The capacity under outage constraint for "strongest-user-only" SCP receivers in the Wyner linear uplink channel is derived in [35][36] (see [37] for a corresponding single cell setup). [38] consider MCP LMMSE receiver for a finite number of cells version of the Wyner linear model. [23] [22] (see also [39])

introduce the soft-handoff model (according to which the cells are located on a circle and the cell-site antennas are located on the cells' boundaries) and consider MCP for Gaussian and fading channels. The uplink channel of the soft-handoff model with MCP can be viewed as a tap ISI channel analyzed by [40]. The variant of the "multi-receiver" network model which is extended to include MIMO fading channels, is introduced in [41] and is analyzed under asymptotic numbers of receive-transmit antennas setup.

Turning to the downlink channel, [42] apply the results of [43], while focusing on Wyner's linear model. Here, LQ-factorization based linear MCP scheme, combined with DPC is analyzed for an *overall* power constraint. In [44] the problem of transmitter optimization to maximize the downlink sum-rate of a *multiple antenna* cellular system is addressed, but with a more realistic *separate* power constraint per each cell-site. The MCP DPC is also used in [45] [46], where the problem of providing the best possible service to new users joining the system without affecting existing users is addressed. The new users are required to be invisible, interference-wise, to existing users, and the network is referred to as "PhantomNet". MCP for the downlink channel of a Wyner "like" planer model in the presence of fading is considered in [47] under asymptotic number of receive-transmit antennas setup and overall power constraint. See [48] for a downlink capacity analysis where no cell-sites cooperation is assumed, and multiuser detection is employed at the mobile receivers for mitigating co-channel interference, though multiuser cooperation has been considered in [9] in a similar setup. In [49] (see also [50]) a generic framework is proposed for the study of base station cooperation in the downlink, utilizing multi-cell DPC, and a cooperative base station selection procedure. Throughput outage calculations of several cooperative joint transmission schemes, including "zero-forcing" and DPC, are reported in [51]. Bounds to the sum-rate capacity supported by the downlink of the soft-handoff model has been reported in [22][23] under per-cell power constraints. [52] consider multi-cell beamforming under minimum receive signal-to-interference ratio constraints, for a general cellular downlink channel model. In [53], distributed beamforming based on local message passing between neighboring base stations is considered for the Wyner linear model through an equivalent virtual LMMSE estimation problem. Multi-cell ZFBF with simple user selection scheme is considered in [26] for the downlink channel of Wyner's linear model with Gaussian and fading channels.

A brief survey for MCP in cellular uplink and downlink channels and related issues, is provided in [54]. MCP schemes are also considered as part of next-generation cellular wireless systems physical-Layer designs in [55].

References

[1] A. Goldsmith, S. A. Jafar, N. Jindal, and S. Vishwanath, "Capacity limits of MIMO channels," *IEEE Journal on Selected Areas in Communications*, pp. 684–702, Jun. 2003.

[2] S. Vishwanath, N. Jindal, and A. Goldsmith, "Duality, achievable rates, and sum-rate capacity of Gaussian MIMO broadcast channels," *IEEE Transactions on Information Theory*, vol. 49, pp. 2658–2669, Oct. 2003.

[3] H. Weingarten, Y. Steinberg, and S. Shamai (Shitz), "The capacity region of the Gaussian MIMO broadcast channel," in *Proceedings of the 2004 IEEE International Symposium on Information Theory (ISIT'04)*, (Chicago, USA), p. 174, June 27 – July 2, 2004.

[4] A. M. Tulino and S. Verdú, "Random matrix theory and wireless communications," *Foundations and Trends in Communications and Information Theory*, vol. 1, 2004.

[5] S. V. Hanly and P. A. Whiting, "Information-theoretic capacity of multi-receiver networks," *Telecommun. Syst.*, vol. 1, pp. 1–42, 1993.

[6] A. D. Wyner, "Shannon-theoretic approach to a Gaussian cellular multiple-access channel," *IEEE Transactions on Information Theory*, vol. 40, pp. 1713–1727, Nov. 1994.

[7] O. Somekh, B. M. Zaidel, and S. Shamai (Shitz), "Spectral efficiency of joint multiple cell-site processors for randomly spread DS-CDMA systems," in *Proceedings of the 2004 IEEE International Symposium on Information Theory (ISIT'04)*, (Chicago, USA), p. 278, June 27 – July 2, 2004.

[8] O. Somekh, B. M. Zaidel, and S. Shamai (Shitz), "Spectral efficiency of joint multiple cell-site processors for randomly spread DS-CDMA systems." to apear in the IEEE Transactions on Information Theory.

[9] N. Laneman, D. Tse, and G. Wornell, "Cooperative diversity in wireless networks: Efficient protocols and outage behavior," *IEEE Transactions on Information Theory*, vol. 50, pp. 3062–3080, Dec. 2004.

[10] E. Aktas, J. Evans, and S. Hanly, "Distributed decoding in a cellular multiple-access channel," in *Proceedings of the 2004 IEEE International Symposium on Information Theory (ISIT'04)*, (Chicago, Illinois, USA), p. 484, June 27–July 2, 2004.

[11] A. Grant, S. Hanly, J. Evans, and R. Müller, "Distributed decoding for Wyner cellular systems," in *Proceedings of the 2004 Australian Communication Theory Workshop (AusCTW'04)*, (Newcastle, Australia), Feb 4–6, 2004.

[12] S. Verdú, "Spectral efficiency in the wideband regime," *IEEE Transactions on Information Theory*, vol. 48, pp. 1329–1343, June 2002.

[13] A. Lozano, A. Tulino, and S. Verdú, "High-snr power offset in multi-antenna communications," *IEEE Transactions on Information Theory*, vol. 51, pp. 4134–4151, Dec. 2005.

[14] M. Sharif and B. Hassibi, "On the capacity of MIMO broadcast channel with partial side information," *IEEE Transactions on Information Theory*, vol. 51, pp. 506–522, Feb. 2005.

[15] S. Shamai (Shitz) and A. D. Wyner, "Information-theoretic considerations for symmetric, cellular, multiple-access fading channels - Part I," *IEEE Transactions on Information Theory*, vol. 43, pp. 1877–1894, Nov. 1997.

[16] R. M. Gray, "On the asymptotic eigenvalue distribution of Toeplitz matrices," *IEEE Transactions on Information Theory*, vol. IT-18, pp. 725–730, Nov. 1972.

[17] O. Somekh and S. Shamai (Shitz), "Shannon-theoretic approach to a Gaussian cellular multi-access channel with fading," *IEEE Transactions on Information Theory*, vol. 46, pp. 1401–1425, July 2000.

[18] R. Durrett, *Probability: Theory and Examples*. Duxbury Press, 3rd ed., 1991.

[19] M. G. Krein and A. A. Nudelman, *The Markov Moment Problem and External Problems*, vol. 50. Rhode Island: American Mathematical Society, 1977.

[20] D. Tse, "Optimal power allocation over parallel Gaussian channels," in *Proc. International Symposium on Information Theory (ISIT'97)*, (Ulm, Germany), Jun. 1997.

[21] W. Yu and T. Lan, "Minimax duality of Gaussian vector broadcast channels," in *Proceedings of the 2004 IEEE International Symposium on Information Theory (ISIT'2004)*, (Chicago, USA), p. 177, Jun. 27 – Jul. 2 2004.

[22] O. Somekh, B. M. Zaidel, and S. Shamai (Shitz), "Sum-rate characterization of

multi-cell processing," in *Proceedings of the Canadian workshop on information theory (CWIT'05)*, (McGill University, Montreal, Quibec, Canada), Jun. 5–8 2005.

[23] O. Somekh, B. M. Zaidel, and S. Shamai (Shitz), "Sum rate characterization of joint multiple cell-site processing." Submitted to the IEEE Transactions on Information Theory, 2005.

[24] S. N. Diggavi and T. M. Cover, "The worst additive noise under a covariance constraint," *IEEE Transactions on Information Theory*, vol. 47, pp. 3072–3081, Nov. 2001.

[25] T. Yoo and A. Goldsmith, "Optimality of zero-forcing beam forming with multiuser diversity," in *Proceedings of the ICC 2005 Wireless Communications Theory (ICC2005)*, (Seoul, Korea), May 16–20 2005.

[26] O. Somekh, O. Simeone, Y. Bar-Ness, and A. M. Haimovich, "Distributed multi-cell zero-forcing beamforming in cellular downlink channels," in *Proceedings of Globecom 2006*, 2006.

[27] O. Simeone, O. Somekh, Y. Bar-Ness, and U. Spagnolini, "Low-SNR analysis of TDMA cellular systems with cooperative base stations and mobiles." Submitted, 2006.

[28] S. Shamai (Shitz) and A. D. Wyner, "Information-theoretic considerations for symmetric, cellular, multiple-access fading channels - Parts I & II," *IEEE Transactions on Information Theory*, vol. 43, pp. 1877–1911, Nov. 1997.

[29] B. M. Zaidel, S. Shamai (Shitz), and S. Verdú, "Multi-cell uplink spectral efficiency of coded DS-CDMA with random signatures," *IEEE Journal on Selected Areas in Communications*, vol. 19, pp. 1556–1569, Aug. 2001. See also: — "Spectral Efficiency of Randomly Spread DS-CDMA in a Multi-Cell Model," Proceedings of the 37th Annual Allerton Conference on Communication, Control and Computing, Monticello, IL, pp. 841–850, Sept. 1999.

[30] B. M. Zaidel, S. Shamai (Shitz), and S. Verdú, "Multi-cell uplink spectral efficiency of randomly spread DS-CDMA in Rayleigh fading channels," in *Proceedings of the 6th International Symposium on Communication Techniques and Applications (ISCTA'01)*, (Ambleside, UK), pp. 499–504, July 15 – 20, 2001. See also: —, "Random CDMA in the multiple cell uplink environment: the effect of fading on various receivers," Proceedings of the 2001 IEEE Information Theory Workshop, Cairns, Australia, Sept. 2–7, 2001, pp. 42–45.

[31] H. Dai and V. H. Poor, "Asymptotic spectral efficiency of multicell MIMO systems with frequency-flat fading," *IEEE Transactions on Signal Processing*, vol. 51, pp. 2976–2988, Nov. 2003.

[32] O. Shental, A. J. Weiss, N. Shental, and Y. Weiss, "Generalized belief propagation receiver for near-optimal detection ot two-dimensional channels with memory," in *Proceedings of the 2004 Information Theory Workshop (ITW'04)*, (San Antonio, Texas, USA), October 24-29, 2004.

[33] B. L. Ng, J. Evans, S. Hanly, and A. Grant, "Distributed linear multiser detection in cellular networks," in *Proceedings of the 2004 Australian Communication Theory Workshop (AusCTW'04)*, (Newcastle, Australia), Feb 4–6, 2004.

[34] O. Shental, N. Shental, S. Shamai (Shitz), I. Kanter, A. J. Weiss, and Y. Weiss, "Finite-state input two-dimensional gaussian channels with memory: Estimation and information via graphical models and statistical mechanics." Submitted to the IEEE trans. on Information Theory, 2006.

[35] B. M. Zaidel, S. Shamai (Shitz), and S. Verdú, "Impact of out-of-cell interference on strongest-users-only CDMA detectors," in *Proceedings of the International Symposium on Spread Spectrum Techniques and Applications (ISSSTA'02)*, vol. 1, (Prague, Czech Republic), pp. 258–262, Sep. 2–5 2002.

[36] B. M. Zaidel, S. Shamai (Shitz), and S. Verdú, "Outage capacities and spectral efficiencies of multiuser receivers in the cdma cellular environment." Submitted to the IEEE trans. on Wireless Communications, 2006.

[37] S. Shamai (Shitz), B. M. Zaidel, and S. Verdú, "Strongest-users-only detectors for randomly spread CDMA," in *Proceedings of the 2002 IEEE International Symposium on Information Theory (ISIT'02)*, (Lausanne, Switzerland), p. 20, June 30 – July 5, 2002.

[38] B. L. Ng, J. Evans, S. Hanly, and A. Grant, "Information capacity of Wyners cellular network with LMMSE receivers," in *Proceedings of the IEEE International Conf. on Communications (ICC'04)*, (Paris, France), 2004.

[39] Y. Lifang and A. Goldsmith, "Symmetric rate capacity of cellular systems with cooperative base stations," in *Proceedings of Globecom 2006*, 2006.

[40] A. Narula, *Information Theoretic Analysis of Multiple-Antenna Transmission Diversity.* PhD thesis, Massachusetts Institute of Technology (MIT), Boston, MA, June 1997.

[41] D. Aktas, M. N. Bacha, J. Evans, and S. Hanly, "Scaling results on the sum capacity of multiuser MIMO systems," *Submitted to the IEEE Trans. Inform. Theory*, 2004.

[42] S. Shamai (Shitz) and B. M. Zaidel, "Enhancing the cellular downlink capacity via co-processing at the transmitting end," in *Proceedings of the IEEE 53rd Vehicular Technology Conference (VTC 2001 Spring)*, vol. 3, (Rhodes, Greece), pp. 1745–1749, May 6–9 2001.

[43] G. Caire and S. Shamai (Shitz), "On the achievable throughput of a multi-antenna Gaussian broadcast channel," *IEEE Transactions on Information Theory*, vol. 49, no. 7, pp. 1691–1706, 2003.

[44] S. A. Jafar and A. J. Goldsmith, "Transmitter optimization for multiple antenna cellular systems," in *Proceedings of the 2002 IEEE International Symposium on Information Theory (ISIT'02)*, (Lausanne, Switzerland), p. 50, Jun. 30 – Jul. 5 2002.

[45] H. Viswanathan, S. Venkatesan, and H. Huang, "Downlink capacity evaluation for cellular networks with known interference cancellation," *IEEE Journal on Selected Areas in Communications*, vol. 21, pp. 802–811, Jun. 2003.

[46] S. A. Jafar, G. Foschini, and A. J. Goldsmith, "Phantomnet: Exploring optimal multicellular multiple antenna systems," *EURASIP Journal on Applied Signal Processing, Special Issue on MIMO Communications and Signal Processing*, pp. 591–605, May 2004.

[47] H. Huang and S. Venkatesan, "Asymptotic downlink capacity of coordinated cellular networks," in *Proceedings of Asilomar Conf. Signals, Syst., and Comput.*, (Pacific Grove, CA), 2004.

[48] H. Dai, A. F. Molisch, and H. V. Poor, "Downlink capacity of interference-limited MIMO systems with joint detection," *IEEE Transactions on Wireless Communications*, vol. 3, pp. 442–453, Mar. 2004.

[49] H. Zhang, H. Dai, and Q. Zhou, "Base station cooperation for multiuser MIMO: Joint transmission and BS selection," in *Proceedings of the Conference on Information Sciences and Systems (CISS'05)*, (Baltimore, Maryland, USA), Mar. 16–18 2005.

[50] H. Zhang, H. Dai, and Q. Zhou, "Base station cooperation for multiuser MIMO: Joint transmission and bs selection," in *Proceedings of the 2004 Conference on Information Sciences and Systems (CISS'04)*, (Princeton University, Princeton, NJ), Mar. 17 – 19, 2004.

[51] G. Foschini, H. C. Huang, K. Karakayali, R. A. Valenzuela, and S. Venkatesan, "The value of coherent base station coordination," in *Proceedings of the 2005 Conference on Information Sciences and Systems (CISS'05)*, (John Hopkins University, Baltimore, ML), Mar. 16 – 18, 2005.

[52] A. Ekbal and J. M. Cioffi, "Distributed transmit beamforming in cellular networks," in *Proceedings of the ICC 2005 Wireless Communications Theory (ICC'05)*, (Seoul, Korea), May 16–20 2005.

[53] B. L. Ng, J. S. Evans, and S. V. Hanly, "Transmit beamforming with cooperative base stations," in *Proceedings of the IEEE International Symposium on Information Theory (ISIT'05)*, (Adelaide, Australia), Sep. 4–9 2005.

[54] S. Shamai (Shitz), O. Somekh, and B. M. Zaidel, "Multi-cell communications: An information theoretic perspective," in *Proceedings of the Joint Workshop on Communications and Coding (JWCC'04)*, (Donnini (Florence), Italy), Oct. 14–17 2004.

[55] G. J. Foschini, H. C. Huang, S. J. Mullender, S. Venkatesan, and H. Viswanathan, "Physical-layer design for next-generation cellular wireless systems," *Bell Labs Technical Journal*, vol. 10, no. 2, pp. 157–172, 2005.

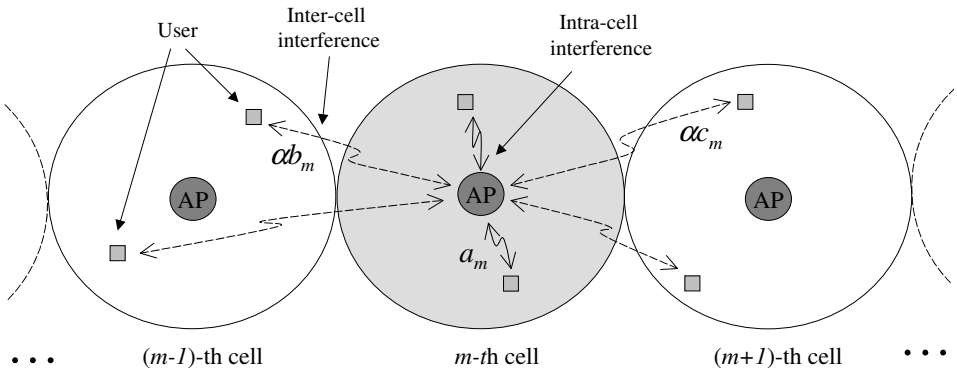

Figure 1.1: Wyner's linear model.

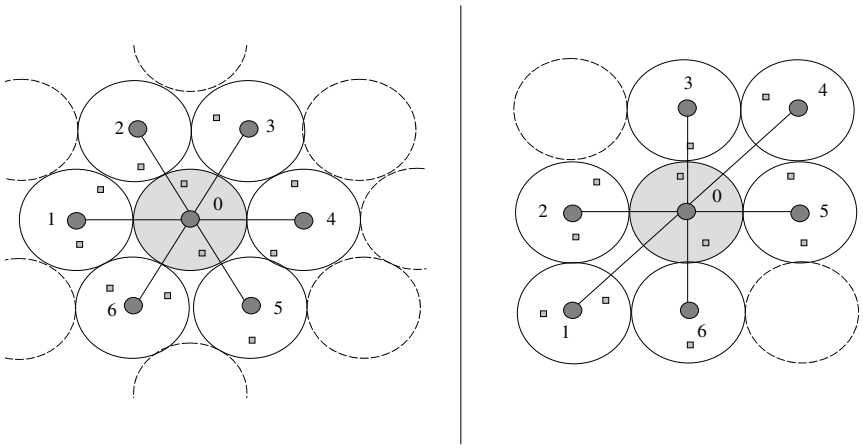

Figure 1.2: Wyner's planar model.

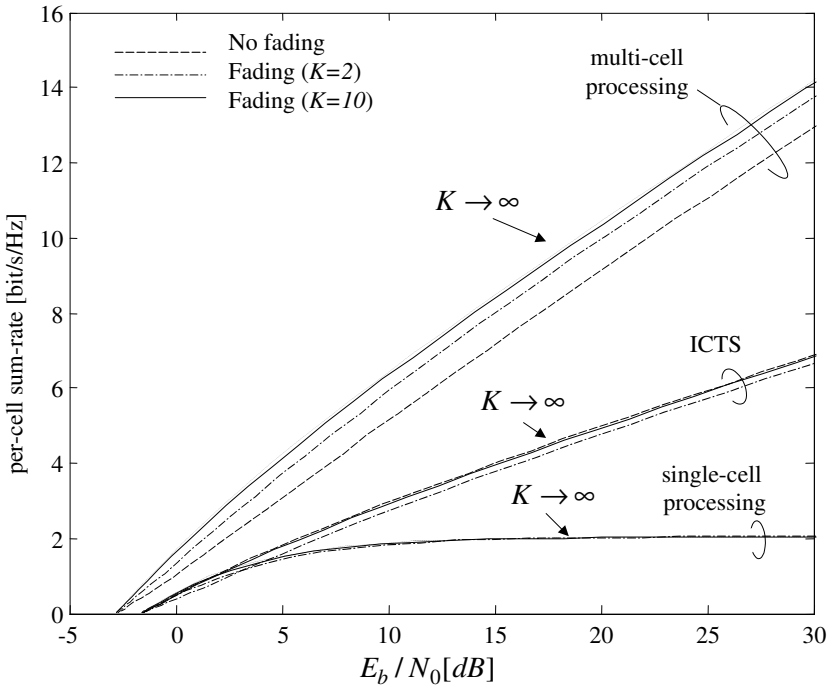

Figure 1.3: Spectral efficiencies versus E_b/N_0 in Wyner's uplink channel ($\alpha = 0.4$).

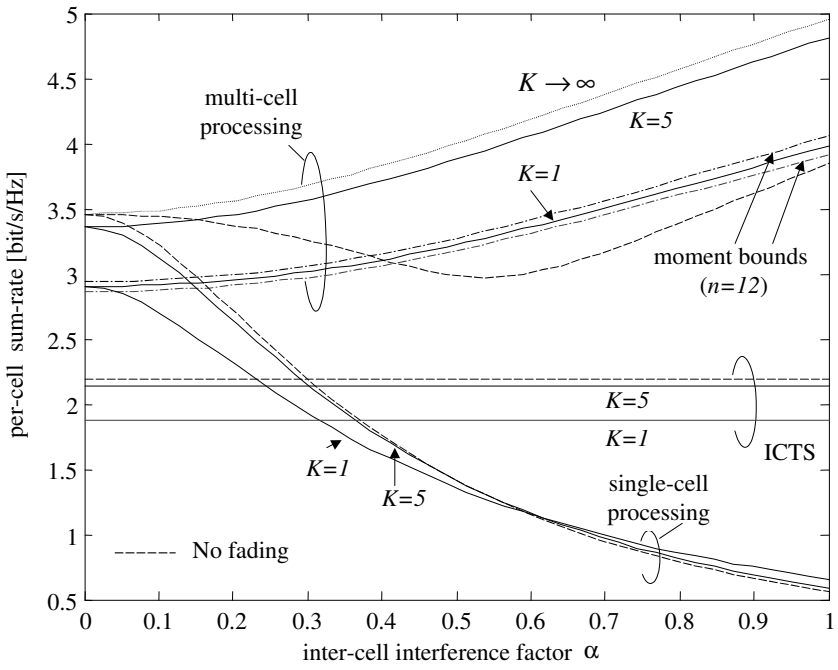

Figure 1.4: Per-cell sum-rates versus inter-cell interference factor α in Wyner's uplink channel ($\bar{P} = 10dB$).

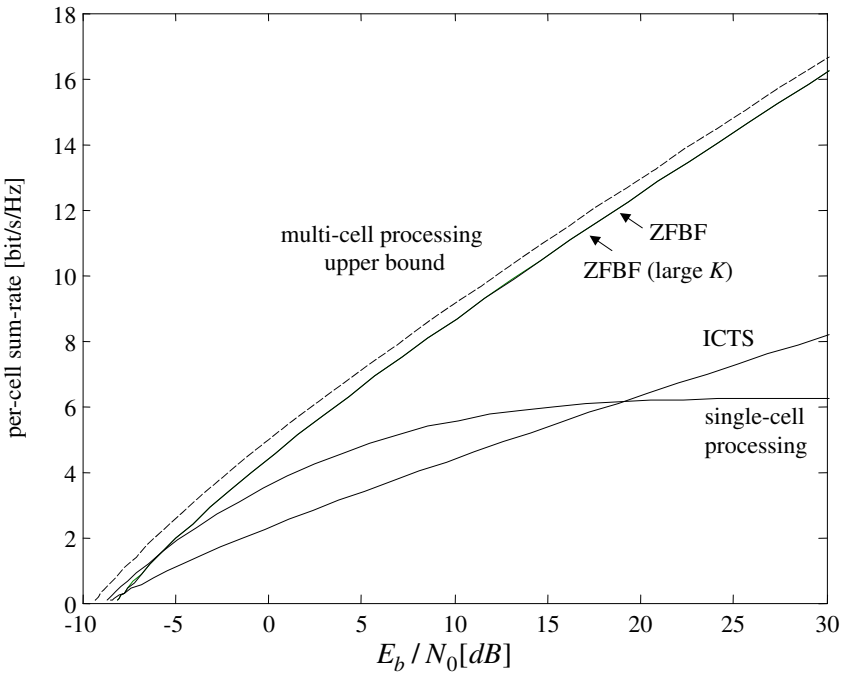

Figure 1.5: Per-cell sum-rates versus E_b/N_0 in Wyner's downlink channel ($K = 100$, $\alpha = 0.4$).

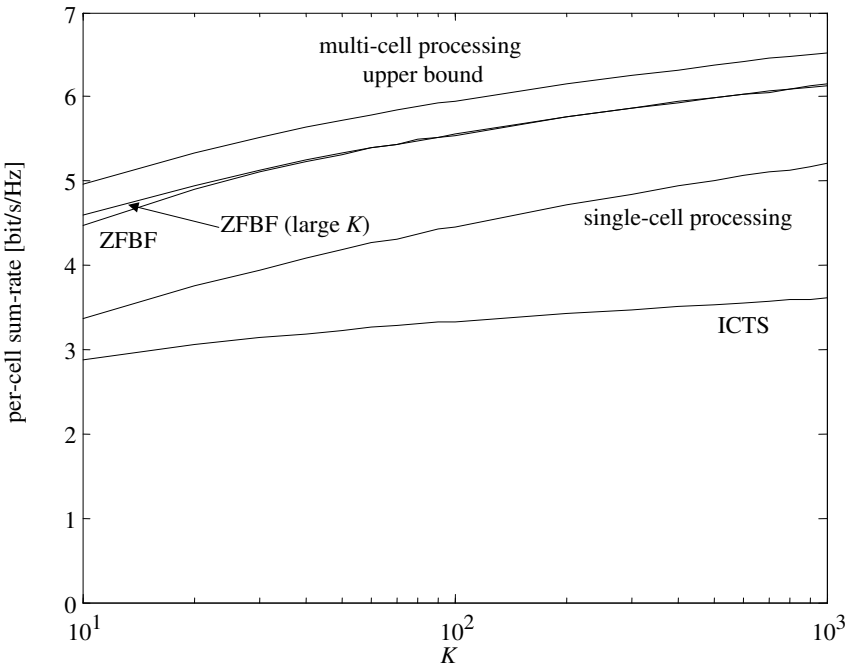

Figure 1.6: Sum-rate versus number of users per-cell K in Wyner's downlink channel ($\alpha = 0.4$, $\bar{P} = 10dB$).

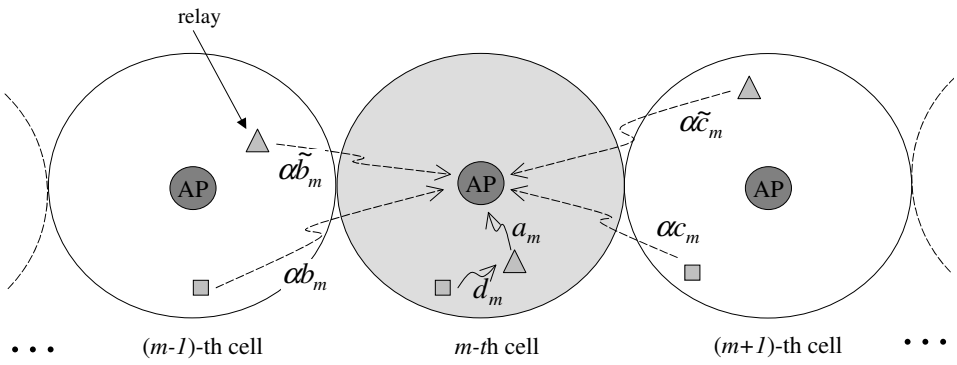

Figure 1.7: Wyner's linear model with cooperation among terminals.

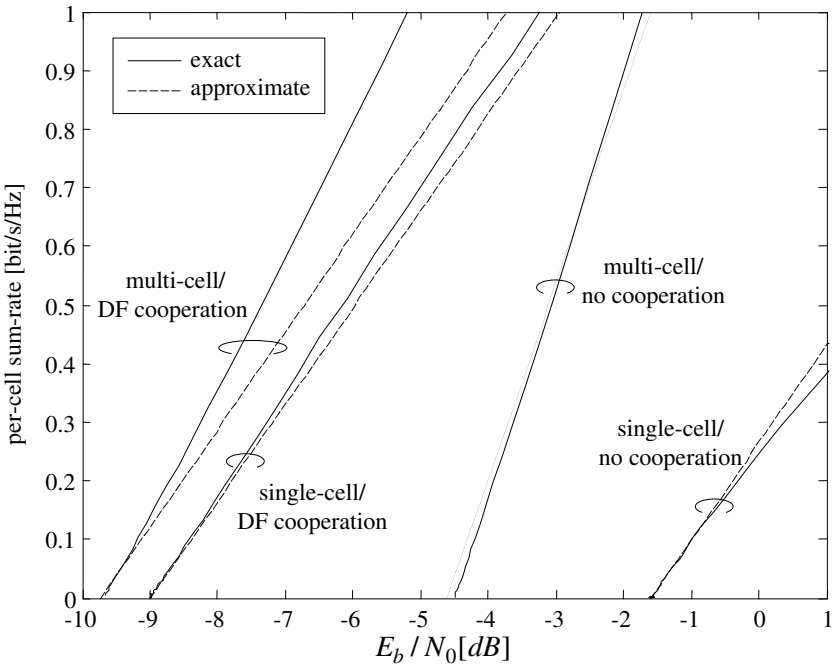

Figure 1.8: Per-cell ergodic rates of different schemes with or without cooperation between either BSs or MTs versus E_b/N_0 ($\alpha^2 = -3$ [dB], $\beta^2 = 20$ [dB], $\gamma^2 = 10$ [dB]). The plot compares the exact achievable rates with the low-SNR approximation (1.1).